Annals of Nuclear Energy 192 (2023) 109941

Contents lists available at ScienceDirect

Annals of Nuclear Energy

journal homepage: www.elsevier.com/locate/anucene

Spent Nuclear Fuel passive gamma analysis and reproducibility: Application to SKB-50 assemblies

Virginie Solans [a,*], Henrik Sjöstrand [a], Peter Jansson [a], Peter Schillebeeckx [b], Sophie Grape [a], Erik Branger [a], Anders Sjöland [c,d]

[a] Uppsala University, Sweden
[b] European Commission, Joint Research Center (JRC), Belgium
[c] Swedish Nuclear Fuel and Waste Management Company (SKB), Sweden
[d] Lund University, Sweden

ARTICLE INFO

Keywords:
SNF
SKB-50
Gamma measurements
Reproducibility

ABSTRACT

This work studies the reproducibility of passive gamma spectroscopy measurements for spent nuclear fuels (SNFs). The fifty assemblies used for this study span over a variety of initial enrichments, burnups, and cooling times. These SNFs have been measured in two different gamma axial measurement campaigns. The net peak counts are determined for Cs-137, Eu-154 and Cs-134. Furthermore, a sensitivity analysis of the relative position of the SNF and the detector is performed. Most importantly, this work describes a methodology using an intrinsic self-calibration procedure that can be used to compare the relative activities of the radionuclides without the need for detailed knowledge about the measurement set-up and its properties. The reproducibility of the Cs-137 net peak count rate ranges between 2% and 4%. Systematic reproducibility of the ratio of Eu-154 and Cs-134 to Cs-137 is between 0,4% - 5 % using the intrinsic self-calibration method.

1. Introduction

On January 27th 2022, the Swedish government approved the application to construct the final disposal of spent nuclear fuel (SNF) at Forsmark in Sweden, as proposed by the Swedish Nuclear Fuel and Waste Management Company (SKB). SKB has chosen direct disposal, where the SNFs will be encapsulated in copper canisters and placed in a geological repository. The application by SKB includes extensive safety assessments aiming to ensure the safe storage of the SNFs over long periods of time, and these assessments include limits on, for instance, criticality and decay heat in the final storage. Decay heat especially is a safety criteria because the temperature at the host rock needs to be limited in order to avoid irreversible structural changes to the host rock and the integrity of the clay buffer around the copper canister (Solans et al., 2021a). These safety parameters will be estimated with detailed calculations for each specific SNF before encapsulation using state-of-the-art codes. Part of the EURAD project (Caruso et al., 2022) (European Joint Program on Radioactive Waste Management), which this work is included in, aims at improving predictions of safety parameters by depletion codes (Jansson et al., 2022). SKB plans to perform measurements to validate predictions by the codes in connection to the encapsulation. Gamma measurements can be used to estimate the gamma dose which is one important safety parameter. Additionally, gamma spectroscopy can be used to indirectly estimate other safety parameters such as decay heat via the Cs-137 content in the SNF (Jansson et al., 2020) or the fuel parameters (burnup, initial enrichment and cooling time (Vaccaro et al., 2016)). Techniques for the verification of the fuel parameters are also important from a safeguards perspective.

The measurements at the encapsulation facility will be performed over several decades, and it is possible that the measurement set-up might change during that time. For instance, gamma detectors or other pieces of equipment may need to be replaced over the years. It is hence crucial to evaluate the consistency and reproducibility of data between measurement campaigns.

In this work, we analyze data from different gamma-spectroscopic measurement campaigns to study the reproducibility of the gamma-ray activity determination, to evaluate if results from different measurements using different setups can be reliably compared. Indeed there have been multiple measurement campaigns on SNF at Clab (central interim storage for SNF), in Sweden. However, the consistency of results between campaigns has not been evaluated before. Experimental measurement data from SNF is scarce, and repeated measurement of the same SNFs is even more scarce. However, the so-called SKB-50 fuel,

* Corresponding author.
E-mail address: virginie.solans@physics.uu.se (V. Solans).

https://doi.org/10.1016/j.anucene.2023.109941
Received 26 January 2023; Received in revised form 15 April 2023; Accepted 21 May 2023
Available online 12 June 2023

selected in 2013–2014, comprising 25 BWR and 25 PWR SNFs from the Swedish nuclear reactors, is spanning the range of fuel parameters initial enrichment, burnup, cooling time expected to be encountered during encapsulation and geological storage. It constitutes a unique set of SNFs that have been repeatedly measured by multiple instruments over many years (Jansson et al., 2020; Vaccaro et al., 2016; Trahan et al., 2020), to develop techniques to be used for SNFs characterization before encapsulation and final storage. The collected data also offers a unique opportunity to evaluate the reproducibility of gamma spectroscopy of SNF.

Two of the dedicated SKB-50 gamma measurement campaigns performed at Clab are analyzed in this paper (more details in the next section). In this work, the net peak counts of Cs-137 (662 keV), Cs-134 (605, 796, 1365 keV), and Eu-154 (996, 1004, 1274, 1596 keV), or ratios of these peaks, are estimated and compared between the different campaigns. The selection of the radionuclides in the study is based on considerations regarding half-lives, branching ratios, and gamma-ray energies and is identical to that in Hellesen et al. (2017). It is expected that for SNFs with cooling times between 10 and 20 years, the gamma-ray peaks from Cs-137, Cs-134 and Eu-154 should be detectable for most of the SNFs. Some peaks may however be too small to be reliably detected for certain SNFs. In most of the results presented, it is the ratio of Eu-154 and Cs-134 over Cs-137 that will be reported, as it prevents systematic biases coming from the uncertainty on the position of the SNF in the measurement set-up. These ratios are also good burnup indicators. Since the net peak counts depend on the measurement conditions, which vary between the measurement campaigns, an intrinsic self-calibration method is developed and used to estimate the relative activities of the three radionuclides. Both ratios of net peak counts and relative activities of the different radionuclides are investigated to determine the consistency between results from the campaigns.

This paper is structured as follows: Section 2 presents the different data sets used in this work. Section 3 details the different methods used in this work. Section 3.1 details the algorithm used to select the recorded events and measurement time when using an axial gamma scan. In Section 3.2 the net peak counts are determined for the eight gamma-ray energies belonging to the three studied radionuclides (Cs-137, Eu-154, Cs-134) in the two axial measurement campaigns. Section 3.3 explains the methodology for the intrinsic self-calibration and Section 3.4 explains the uncertainty calculation for this method. The results of the work are in Section 4. The comparison of results from the different campaigns is detailed in Section 4.1. A sensitivity analysis on the position of the SNF is found in Section 4.2. The results of the relative activity of the two axial campaigns are in Section 4.3 with the corresponding uncertainties in Section 4.4. Finally, a discussion on the results in Section 5 and a conclusion of the work in Section 6 are presented. In the appendix, tables presenting the measured count rates and the results of the intrinsic self-calibration on campaigns 1 and 2 are available.

2. Presentation of the data

In this paper two of the dedicated SKB-50 gamma measurement campaigns performed at Clab are analyzed. A summary of the measurement campaigns considered in this work is presented in this section.

The SKB-50 SNFs were measured in 2014. This measurement campaign is referred to as campaign 1 in this paper. During this campaign, the SKB-50 SNFs were axially scanned, meaning that the SNFs moved vertically from below the detector to above the detector and down again. The detector recorded the count rates continuously, giving information about the activity in the SNF at different heights. Information about the measurement set-up, detector, and acquisition system for this campaign can be found in Vaccaro et al. (2016).

In the second gamma measurement campaign, taking place in both 2016 and 2019, the SKB-50 SNFs were again axially scanned. The raw data are available in Jansson et al. (2020). For this campaign, details on the measurement set-up, detector, and acquisition systems are in Jansson et al. (2020). The PWR SNFs were measured in 2016, and the BWR SNFs were measured in 2019. This measurement campaign is referred to as campaign 2. One important difference is that in campaign 2, a Cs-137 calibration source was located between the SNF and the detector inside the collimator (more details and explanation about the Cs-137 source can be found in Bengtsson et al., 2021). The calibration source is treated as a background in this work.

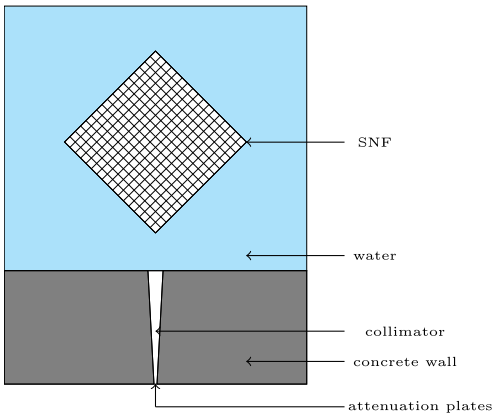

Fig. 1. Scheme of the measurement set-up from above. The squared fuel assembly is surrounded by water (blue), and the concrete surrounding the collimator is shown in gray. Note that the figure is not to scale, as the collimator is considerably longer than the diameter of the fuel assembly. The width of the wall, including the collimator, is 2 m long, and the distance between the SNF and the pool wall is approximately half a meter. The SNF has one corner facing the collimator opening, as was intended in the measurements, but in fact, the SNF can rotate with respect to the collimator and also move vertically. The detector is located in the room after (below in figure) the attenuation plates.

In all measurements, the SNFs are oriented with one corner facing the detector, see Fig. 1 because this reduces the distance between the SNF and the detector. The Table A.12 (in the appendix) shows the different corners that have been measured in the campaigns described above. By measuring the different corners of the SNF it is possible to estimate whether the SNF was asymmetrically burned in the reactor and hence experienced a burnup gradient. That would be seen as a variation in net peak counts, depending on what corner is facing the detector (Jansson et al., 2016).

The top of the SNF is located around 10 m below the water surface (Vaccaro et al., 2016) at the beginning of the measurements. A steel plate separates the pool and the collimator opening, and the collimator extends through the wall to the adjacent room, where the measurement equipment is placed. The distance between the SNF and the pool's wall is about half a meter (Vaccaro et al., 2016). The air-filled collimator hole is located in the concrete wall, the width's wall is 190 cm long (Jansson et al., 2016). The attenuation plates are placed between the collimator and an HPGe detector, in the measurement equipment room. The attenuation plates aim at reducing the count rate and therefore allow for better control of the dead-time in the detector. Several different attenuation plates are available for use, made of copper, lead, stainless steel or aluminium, to reduce the gamma rays of different energies. Different sets of attenuation plates have been used throughout the campaigns, as detailed in Table 1. It must be noted that even if the number of attenuation plates is known and detailed in Table 1, some information is missing from the authors. For instance, the type of stainless steel (SS) used, and thus its density and the attenuation coefficient, are not known. The assumptions used are detailed in Section 3.2. A constant speed for the SNF elevator in the pool is assumed for each direction.

Table 1
List of attenuation plates used in the different campaigns.

	Campaign 1		Campaign 2	
	BWR	PWR	BWR	PWR
Year	2014	2014	2019	2016
Attenuation plates	None	8 mm Pb +21 mm SS +3 mm Al +1 mm Cu	10 mm Pb +1 mm Cu	Various combinations (None or 4 mm Pb +1 mm Cu or 10 mm Pb +1 mm Cu)
Reference work	This work	This work	Jansson et al. (2020)	Jansson et al. (2020)

3. Methodology

3.1. Data selection for axial gamma scans

For both campaigns 1 and 2, the net peak counts for a number of gamma-ray energies are determined from the raw data using a two-step process. The first step involves event selection in order to select only counts when the SNF is fully in front of the detector, and that step is detailed in this section. The second step concerns the determination of the net peak counts, which is detailed in Section 3.2.

In the axial scans, time stamped list mode data is collected, meaning information on both detected gamma-rays and their detection time are recorded. That information can be used to determine when the fuel assembly is located in front of the collimator. This section describes an algorithm to select only the data when the assembly is only fully in front of the detector. In this work, only full-energy count rate peak areas are considered, therefore it will referred to as net peak count for the rest of the work.

The list mode data for the gamma spectroscopic measurements data performed for campaigns 1 and 2 (Jansson et al., 2020) is grouped into batches. Each batch is associated with a live-time. When the SNF is in front of the detector, the count rate is high and the detector is not able to record all events due to the dead-time associated with the electronics. By using the information on the live-time for each batch, the counts per live-time (in counts per second [cps]) are inferred. By doing so, a dead-time correction for the ADC is obtained.

Fig. 2 displays the count rate per live-time (in cps) from one PWR SNF and the Cs-137 source as a function of the live-time. One can observe that most of the measurement time is spent recording background. Thus the measurement time and the batches used to compute the SNF's average count rate should be adjusted to account only for the time spent by the SNF in front of the detector. A time selection algorithm for this purpose is described in detail in Jansson et al. (2016). The idea of that algorithm is to divide the measurement live-time of one SNF into five groups depending on the relative position of the SNF and detector. Group 1 (see Fig. 2) represents events recorded while the SNF is below the field-of-view of the detector. Group 2 contains events recorded when the SNF is in front of the detector and moving upwards. Group 3 contains events when the SNF is above the detector. Group 4 corresponds to events when the SNF is again in the field-of-view of the detector, now moving downwards. The 5th group contains events recorded when the SNF is again below the detector. The analysis will only make use of data from groups 2 and 4. In order to separate these groups, a count rate threshold is initially set to 1 count per second (cps). For every second during the measurement, the count rate is computed. Groups of events are created each time a transition is above or below the threshold. If the final number of groups is larger than five, the threshold is increased by one cps until five groups are reached.

Fig. 2 displays the count rate as a function of the live-time. The red lines correspond to the distinctions between each group according to the algorithm described above. Fig. 2 clearly shows that each SNF is in front of the detectors at two occasions, once when it is moving upwards, and once when it is moving downwards.

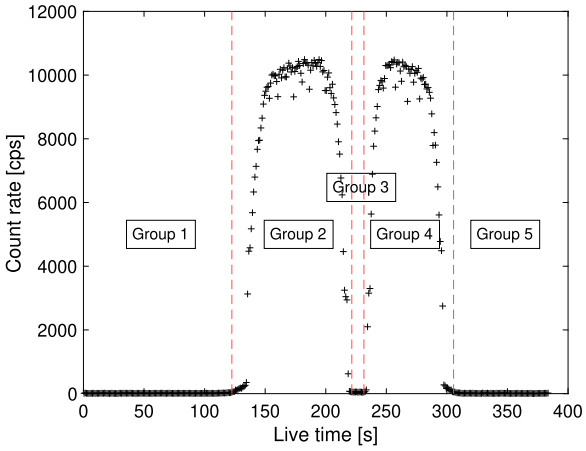

Fig. 2. In black: total count rate for the SNF denoted PWR01, corner 135 using the notation in Jansson et al. (2020). In red: time limitation between each group with the algorithm described in Jansson et al. (2016).

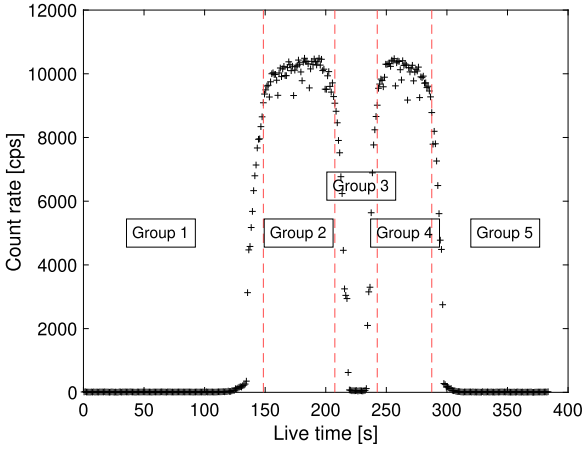

Fig. 3. In black: total count rate for the SNF denoted PWR01, corner 135 using the notation in Jansson et al. (2020). In red: time limitation between each group with the updated algorithm used in this paper.

The time-frames presented in Fig. 2 can be modified to also exclude data when the SNF is assumed to be only partially in front of the detector through the collimator. Therefore, the time-selection algorithm is further improved in this work. Indeed, the threshold originally set to 1 cps and increased is now set to the highest count rate and then decreased until the five groups are formed. Fig. 3 displays the new group limitation with the red lines. Using this method and by considering events in groups 2 and 4, it is possible to create an energy-resolved gamma spectrum for each SNF by summing all counts within the time window. It is the average spectrum along the SNF length for one corner. The same algorithm has been applied to both campaigns, so the same region of burnup is compared.

Table 2
Gamma-ray energies of interest depending on their radionuclides, branching ratio (BR) and radionuclides' half-life.

Radionuclides	Cs-137	Eu-154	Eu-154	Eu-154	Eu-154	Cs-134	Cs-134	Cs-134
Energy [keV]	662	996	1004	1274	1596	605	796	1365
BR [%]	85.1	10.6	17.91	35.19	1.798	97.62	85.53	3.014
Half-life [y]	30.07	8.593	8.593	8.593	8.593	2.065	2.065	2.065

3.2. Net peak count

The method used to compute the net peak counts of selected gamma-ray energies in this work is described in Solans et al. (2021b). The method uses numerical integration to determine the net peak area, with the background described by a complementary error function. The method used in this work is referred to as NI_E (Numerical integration fitting background using only edge channels) in Solans et al. (2021b). To be consistent with the rest of the paper, net peak area will be described as net peak count, as the area is divided by the measurement time.

The methodology described to obtain the net peak counts is applied to the data from campaigns 1 and 2 for all eight peaks of interest, given in Table 2, in all measurements where a selected corner is facing the detector. The list of the corners measured for each SNF during the different measurement campaigns is listed in Table A.12. The results are summarized in Tables C.15 and C.16. The NaN values refer to cases when the net peak count rate is close to zero, and thus not detectable.

Campaign 1 and 2 data is corrected for the use of attenuation plates (except Table C.15 in the appendix) as detailed in Table 1 by using the exponential attenuation law (details can be found page 53 of Knoll, 1989). However, in campaign 2, different sets of attenuation plates were used, and thus different attenuation functions were used in the analysis. The attenuation coefficients for Cu, Al and Pb are taken from Seltzer (1995). The composition and density of the stainless steel attenuation plates used in campaign 1 are unknown to the authors and thus a density of 8 g/cm^3 is assumed, and the attenuation coefficient in Sadawy and El Shazly (2019) is used.

All the figures and results in this work are corrected for the decay time to allow the results from the different campaigns to be directly compared. The Table C.16 in the appendix, which contains the net peak counts for campaign 2, is not corrected for the decay time between 2014 and 2016–2019 in order to let the reader reuse the Tables C.15 and C.16 for future study.

3.3. Intrinsic self-calibration

In order to be able to compare net peak counts in gamma peaks between different measurement campaigns, one must either ensure that the measurement conditions are the same, or compensate for the differences, such as the use of different detectors, different attenuation plates etc. One possible solution along the line of compensating for factors that are not identical, is to perform an intrinsic self-calibration for each SNF that takes into account the detector efficiency, geometry, attenuation plates, etc. This allows a ratio of activities to be calculated. In this work, the aim is to look at the ratio of Eu-154 and Cs-134 over Cs-137. Similar methods were developed and explained in Favalli et al. (2016), Sampson et al. (2003).

In this work, such an intrinsic self-calibration is performed. The advantage of determining the ratio of radionuclides is that there is no need to know what the absolute attenuation coefficients are or what the absolute detector efficiency (Bengtsson et al., 2021) is. The ratio of activity is also sufficient for most applications (Hellesen et al., 2017).

The idea of an intrinsic self-calibration is to use the emitted radiation to assess the attenuation in the measurement set-up. Looking at a single radionuclide that emits gamma-rays of multiple energies, the relative source strength of each gamma-ray energy is known through the branching ratio (BR). Thus, by comparing the relative detected activities to the known relative source activities, the gamma attenuation as a function of energy can be assessed. By combining the data from multiple radionuclides, the attenuation can be assessed at additional energies, decreasing the uncertainty. The intrinsic self-calibration methodology is described as follows :

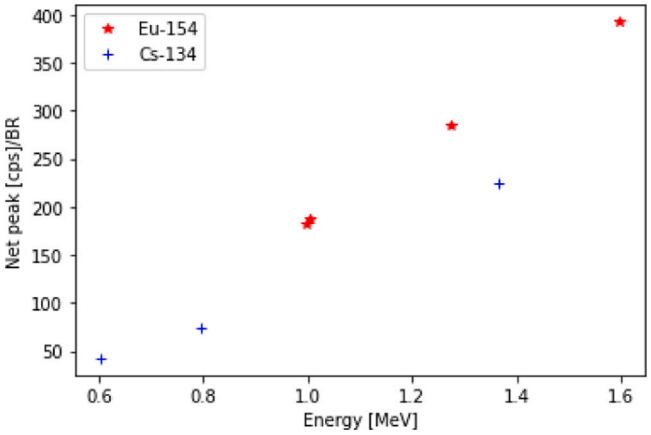

Fig. 4. Measured net peak counts divided by their BR for selected Cs-134 and Eu-154 gamma-ray energies.

• First, one must identify the gamma-ray energies to be used in the intrinsic self-calibration. A set of radionuclides that emit detectable gamma-rays of multiple energies that span over a large energy range is required. In long-cooled SNF, only a few gamma-ray peaks are visible. Typically Eu-154 and Cs-134 have multiple energies peaks that span over a large energy range, and reasonable decay-time. Hence can be used for intrinsic self-calibration. In this work, the gamma peaks at 605, 796 and 1365 keV for Cs-134 and 996, 1004, 1274 and 1596 keV for Eu-154 were selected because they can be found in a gamma-ray spectrum from long-cooled SNFs. It is also necessary to normalize the net peak counts of a particular peak to the BR associated with that particular emission. Hence, the net peak counts become independent of the BR, but are still dependent on the activity and the geometric efficiency. In Fig. 4, red (Eu-154) and blue (Cs-134) markers show the net peak counts after correcting for the associated BRs for that particular emission.

• In the second step, the dependency of the net peak count on the activity of the different radionuclides is addressed and corrected for. With this type of correction, it is possible to relate the net peak counts from one radionuclide to those of another radionuclide. The system of equations described in Eq. (1) needs to be solved to find the attenuation fit.

The polynomial fit of degree two represents the product between the detector efficiency and the attenuation of the gamma peaks in the different media (water, attenuation plates, air and fuel). After the intrinsic self-calibration has been performed, the relative activity of any gamma emission can be determined. The relative activity relates different emission sources to each other.

$$\begin{cases} C_{Eu-154,i,k}/BR_{Eu-154,i} = (a_k \cdot E_i^2 + b_k \cdot E_i + d_k) \\ C_{Cs-134,i,k}/BR_{Cs-134,i,k} = (a_k \cdot E_i^2 + b_k \cdot E_i + d_k) \cdot R_k \end{cases} \quad (1)$$

In Eq. (1), C is the count rate of a specific peak, BR is the branching ratio associated with the emission and E is the energy of the gamma-ray. The index i describes the different full-energy peaks of Eu-154 and

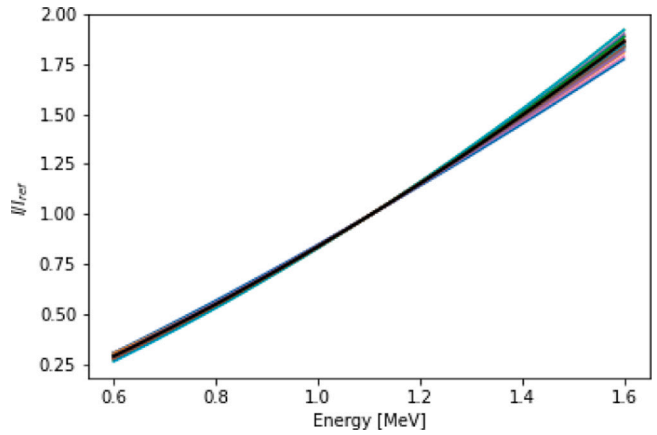

Fig. 5. Intrinsic self-calibration with polynomial fits for the PWR SKB-50 SNFs in campaign 2 in colors and polynomial fit using sum of all net peak counts for the PWR SKB-50 SNFs in campaign 2 in black. To be independent of the SNF's activity, all fits have their intensity (I) normalized to 1 at 1.1 MeV (I_{ref}).

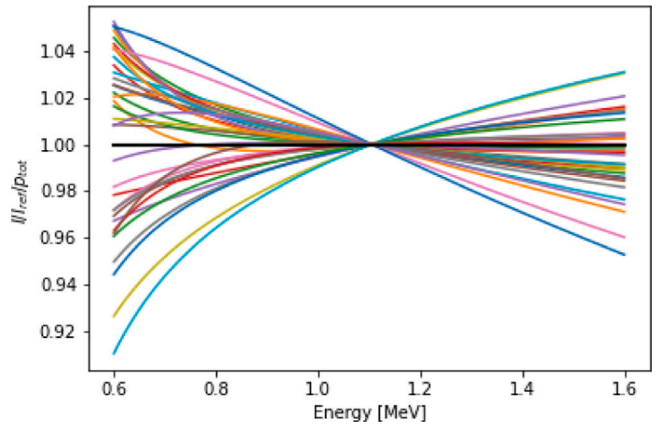

Fig. 6. Intrinsic self-calibration with polynomial fits for the PWR SKB-50 SNFs in campaign 2 in colors divided by the polynomial fit using sum of all net peak counts for the PWR SKB-50 SNFs in campaign 2 (p_{tot} in black). To be independent of the SNF's activity, all fits have their intensity (I) normalized to 1 at 1.1 MeV (I_{ref}).

Cs-134. The index k indicates that the system needs to be solved for each campaign and for BWR/PWR separately. The parameters that need to be determined are a, b, d and R. The parameters a, b and d describe a polynomial of degree two, which represent the product of the different attenuations. The parameter R describes the ratio of activities between Eu-154 and Cs-134 and allows for the removal of the dependency on the activity of the different radionuclides. These four parameters are found using a non-linear least square regression optimization (*curve_fit* from the scipy python package Virtanen et al., 2020).

Fig. 5 shows the polynomial fits used in the intrinsic self-calibration for different SNFs normalized to 1 at 1.1 MeV (the normalization is only for visualization to be able to include all plots in the same figure. Hence, the normalization point at 1.1 MeV is arbitrarily chosen). One can observe that in Fig. 5, the calibration polynomials are quite similar, and the small differences originate in the individual net peak count determinations and their associated uncertainties. By using individual intrinsic self-calibration fits for each fuel assembly, the effect of the positioning of the SNF in the measurement set-up can be taken into account. However, in some cases, there is an insufficient number of peaks in the gamma spectrum to be able to perform the intrinsic self-calibration. In order to remedy this, all the net peak counts for each energy peak have been summed up for each type (BWR or PWR) and each campaign. Therefore, the same intrinsic self-calibration polynomial is applied to all SNFs (PWR and BWR separately), i.e. no individual

Table 3
Values of the global fit for each campaign and each fuel type used in this work.

	Campaign 1		Campaign 2	
	BWR	PWR	BWR	PWR
a_k	0.248	0.532	0.280	0.192
b_k	0.676	−0.171	1.09	0.463
d_k	−0.326	−0.032	−0.4878	−0.181

calibrations have been used. This global fit allows all SNFs to be calibrated, even if individual SNFs may not have sufficiently many peaks to allow an individual intrinsic self-calibration. The term "self" in intrinsic self-calibration is then not entirely appropriate because it is not only information for the studied assembly that is used but also from similar assemblies. However, the term intrinsic self-calibration is still used throughout the paper as it is the common terminology used to describe this type of methodology and the method presented can also be used on individual assemblies. Fig. 5, shows the fit (in black) created using the sum of the net peak counts. The values of the global fit for the two campaigns and for each fuel type are available in Table 3. The global fit also reduced the uncertainty on the net peak when summed. Uncertainties due to the counting statistics leading to systematic uncertainty on the final results, are detailed in Tables 10 and 11. Hence using a global best fit ensures consistency and improved peak count statistics but may introduce some additional errors. There are not believed to be any major unaccounted changes to the experimental set-up within the campaigns. This is also supported by the similar shapes of the intrinsic self-calibration fits shown in Fig. 5. In order to quantify the difference between using individual fits and using the global fit the mean standard calibration is calculated. For campaign 2, the mean standard deviation is 1.2% for the PWRs (Fig. 5) and 2.2% for BWRs. For campaign 1, the mean standard deviation is 1.4% for PWRs and 0.8% for BWRs. Fig. 6, shows the individual fits in colors divided by the global fit. This figure permits better visualize the differences between the global fit and individual fits. For this figure and Fig. 5, the intensities have been divided by the intensity of the fits at 1.1 MeV. This normalization is just to remove the dependency on the activity and thus to show all curves on the same plot. This normalization is not used in any way in the results; it is only used in these figures to show the different curves more easily. The differences between the individual fits and the global fit originate from the lack of statistics in the individual fits but could also come from small geometrical changes or positioning between the SNFs. Indeed, minor changes to the attenuation due to, e.g. SNF bowing or fuel geometry cannot be ruled out, and will not be captured using a global fit. In particular, the polynomial fit has been determined independently of the SNF geometry or the vendor's design. In the case of BWR SNF, only 10 × 10 SNF have been used to determine the polynomial fit, as the 8 × 8 are long-cooled SNF, where Cs-134 is no longer detectable. For PWR SNFs, a mix between 15 × 15 and 17 × 17 SNF is used in the global fit.

Once the polynomial has been determined, by using Eq. (2), it is possible to obtain the relative activities for any radionucleides, which will be Cs-134, Eu-154 and Cs-137 in this work.

$$s_{i,k} = \frac{C_{i,k}}{BR_i \cdot (a_k \cdot E^2 + b_k \cdot E + d_k)} \tag{2}$$

In Eq. (2), i represents the selected energy peak of one of the radionuclides (Cs-137, Eu-154 or Cs-134). k is the index which describes the campaign measurement and for BWR/PWR. s is the count rate after the intrinsic self-calibration, and C is the count rate. The parameters a, b and d are the parameters of the polynomial fit determined in Eq. (1). E is the energy of the full energy peak.

3.4. Uncertainty

The goal of this section is to describe the uncertainties related to the intrinsic self-calibration method. All uncertainties reported in this work are quoted as one sigma.

The uncertainty of the relative activities from the intrinsic self-calibration method is divided between a systematic ($\Delta s_{systematic}$) and a random component (Δs_{random}). For simplicity the uncertainty from random/systematic effect will be call random/systematic uncertainty. The relative activities of two radionuclides are calculated using Eq. (2). The random uncertainty component comes from the Poisson distribution of the gamma count rate and is described in Eq. (3)

$$\Delta s_{random,i,k} = s_{i,k} \cdot \frac{\Delta C_{i,k}}{C_{i,k}} \tag{3}$$

where s is the relative activity described in Eq. (2). C is the net peak count, and ΔC is the uncertainty of the net peak count. The index i describes the full-energy peaks of the different radionuclides. The index k is for the different campaigns and fuel types (BWR or PWR).

The systematic is coming from the uncertainty of the polynomial fit used (p) for the intrinsic self-calibration method. This uncertainty component is calculated using Eqs. (4) and (5).

$$\Delta s_{systematic,i,k} = s_{i,k} \cdot \frac{\Delta p_k(E_i)}{p_k(E_i)} \tag{4}$$

$$\Delta p_k(E) = \sqrt{J(E) \cdot Cov_{tot} \cdot J(E)^T} \tag{5}$$

$$J(E) = \begin{pmatrix} \frac{\partial p_k(E)}{\partial a_k} \\ \frac{\partial p_k(E)}{\partial b_k} \\ \frac{\partial p_k(E)}{\partial d_k} \end{pmatrix} = \begin{pmatrix} E^2 \\ E \\ 1 \end{pmatrix} \tag{6}$$

$$Cov = \begin{pmatrix} \sigma^2_{a_k a_k} & \sigma^2_{a_k b_k} & \sigma^2_{a_k d_k} \\ \sigma^2_{b_k a_k} & \sigma^2_{b_k b_k} & \sigma^2_{b_k d_k} \\ \sigma^2_{d_k a_k} & \sigma^2_{d_k b_k} & \sigma^2_{d_k d_k} \end{pmatrix} \tag{7}$$

where $J(E)$ is the Jacobian of the polynomial fit evaluated at the energy (E), and Cov the covariance matrix obtained with the $curve\_fit$ function of the $scipy$ (Virtanen et al., 2020) python library using default settings, for the polynomial fit p. The diagonal terms of the covariance matrix are the variance of each variable (a_k, b_k and d_k). The off-diagonal terms are the covariance terms between pairs of different variables. The index i describes the full-energy peaks of the different radionuclides. The index k is for the different campaigns and fuel types (BWR or PWR).

For all results reported (including Tables 4 to 9), the weighted mean value and the weighted standard deviation are calculated using weights from the random uncertainty. The weights are calculated using the inverse-variance weighting method (Hartung et al., 2008). The weighted mean is calculated using the following equation:

$$\mu = \frac{\sum_i w_i \cdot R_i}{\sum_j w_j} \tag{8}$$

The weighted standard deviation is calculated using the following equation:

$$Std_{weighted} = \sqrt{\frac{\sum_i w_i (R_i - \mu)^2}{\frac{N-1}{N} \sum_j w_j}} \tag{9}$$

In Eqs. (8) and (9), w are the weights, R is ratio of activities, μ is the weighted mean, and N is the number of measurements taken into account. The index on the weights and ratio of activities represent the different SNF measurements.

4. Results

4.1. Comparison of net peak counts between the two axial scans campaigns

It is possible to compare measurement data from each corner individually for campaigns 1 and 2. This section does not use the intrinsic self-calibration that was detailed in Section 3.3. In this work, the level of agreement between net peak count rates determined from measurements on each corner is evaluated for campaigns 1 and 2. Each result presented in this work, starting from this section, described the ratio of a measurement made in campaign 1 over the same quantity in campaign 2.

The weighted standard deviation of the ratio for all BWR corner measurements is 2.2%, while it is 3.9% for the PWR SNFs for Cs-137. This should be compared with the uncertainty reported in Tables C.15 and C.16. The average uncertainty in the Cs-137 net peak count is 0.2% for both campaigns 1 and 2, as seen in Table C.17. Uncertainties from individual corners are hence typically below 1%, and the weighted standard deviation of 2.2% and 3.9% in the campaigns cannot be explained by the uncertainty due to the peak area determination. Uncertainties related to the set-up (positioning of the SNF, orientation of the SNF e.t.c.) have to be included in the analysis to explain the deviation between the campaigns. A study of the attenuation depending on the relative position of the SNF and the detector for Cs-137 is detailed in Section 4.2. The level of agreement in net peak counts between the measurement campaigns is also dependent on the correction for the attenuation plates. This correction requires detailed information about the plates. In this work, some assumptions about the stainless steel properties were made (such as composition, density, etc.), and this affects the results (see Section 3.2).

Tables 4 and 5 present the weighted mean values and weighted standard deviations of the energy-specific radionuclide ratios in campaign 1 over campaign 2 of the net peak counts for different gamma-peaks. The ratios are calculated for each individual corner. The number of measurements (for each assembly and corner) taken into account in the results is noted in the last column of the tables, as not all radionuclides were measurable for all SNF. The weighted standard deviation ranges between 3% and 9% for Eu-154 and Cs-134, which is in agreement with the uncertainties reported in Tables C.15 and C.16. Table 4 has mean values frequently below 1, which may indicate a systematic difference between the measurement campaigns. The mean weighted values of ratio of the net peaks counts for canpaign 1 over capaign 2 reported in Table 4 are plotted in Fig. 7 depending on the energy of the peaks. It can be observed that there is a trend. It indicated that an attenuation,

Table 4
Weighted mean value and weighted standard deviation of ratio of the net peak area in campaign 1 over that in campaign 2 for the BWR SKB-50 assemblies. Nb is the number of measurements (corner × SNF) taken into account in the ratio.

Nuclide	Energy [keV]	Mean	Std	Nb
Cs-137	662	1.014(3)	0.022(2)	69
Eu-154	996	0.922(7)	0.054(5)	61
Eu-154	1004	0.933(4)	0.033(3)	64
Eu-154	1274	0.913(4)	0.029(2)	69
Eu-154	1596	0.939(8)	0.064(6)	62
Cs-134	605	1.171(21)	0.086(15)	16
Cs-134	796	0.949(5)	0.024(3)	27
Cs-134	1365	0.928(8)	0.041(6)	27

Table 5
Weighted mean value and weighted standard deviation of ratio of the net peak area in campaign 1 over that in campaign 2 for the PWR SKB-50 assemblies. Nb is the number of measurements (corner × SNF) taken into account in the ratio. In this table results cannot be fully trusted, because of the unknowns on the attenuation plates corrections in particular regarding the type of stainless steel used (see Section 3.2).

Nuclide	Energy [keV]	Mean	Std	Nb
Cs-137	662	0.950(4)	0.039(3)	93
Eu-154	996	0.968(5)	0.048(4)	85
Eu-154	1004	0.993(4)	0.041(3)	92
Eu-154	1274	1.098(4)	0.035(3)	93
Eu-154	1596	1.401(7)	0.066(5)	93
Cs-134	605	1.000(8)	0.050(6)	39
Cs-134	796	0.937(4)	0.028(3)	56
Cs-134	1365	1.165(3)	0.022(2)	46

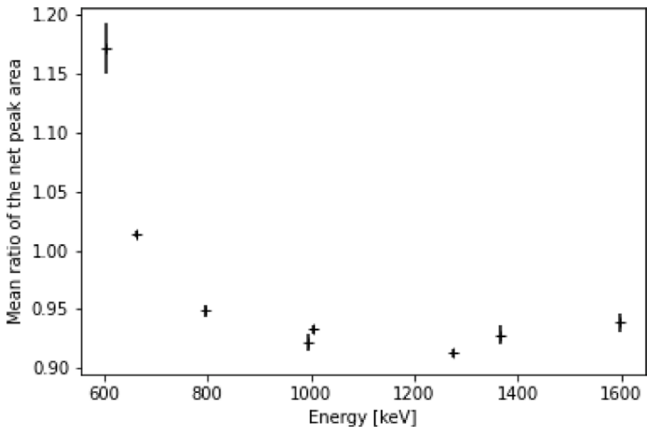

Fig. 7. Weighted mean of ratio of the net peak count in campaign 1 over campaign 2 for BWR SNFs depending on the energy of the peaks.

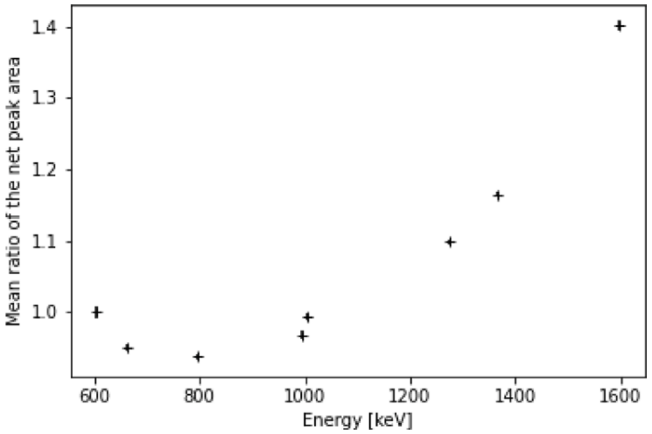

Fig. 8. Weighted mean of ratio of the net peak count in campaign 1 over campaign 2 for PWR SNFs depending on the energy of the peaks.

Table 6
The ratio of campaign 2 over that in campaign 1 of net peak ratios to Cs-137. Results for the BWR SKB-50 assemblies. Column 2: weighted mean values. Column 3: weighted standard deviation. Nb is the number of measurements (corner × SNF) taken into account in the ratio.

BWR	Mean	Std	Nb
996 keV, Eu-154/ 662 keV, Cs-137	0.911(7)	0.054(5)	61
1004 keV, Eu-154/ 662 keV, Cs-137	0.932(5)	0.038(3)	64
1274 keV, Eu-154/ 662 keV, Cs-137	0.908(3)	0.026(2)	69
1596 keV, Eu-154/ 662 keV, Cs-137	0.948(10)	0.081(7)	62
605 keV, Cs-134/ 662 keV, Cs-137	1.165(23)	0.091(16)	16
796 keV, Cs-134/ 662 keV, Cs-137	0.946(4)	0.018(2)	27
1365 keV, Cs-134/ 662 keV, Cs-137	0.923(8)	0.040(5)	27

Table 7
The ratio of campaign 2 over that in campaign 1 of net peak ratios to Cs-137. Results for the PWR SKB-50 assemblies. Column 2: weighted mean values. Column 3: weighted standard deviation. Nb is the number of measurements (corner × SNF) taken into account in the ratio. In this table results cannot be fully trusted, because of the unknowns on the attenuation plates corrections in particular regarding the type of stainless steel used (see Section 3.2).

PWR	Mean	Std	Nb
996 keV, Eu-154/ 662 keV, Cs-137	1.025(5)	0.044(3)	85
1004 keV, Eu-154/ 662 keV, Cs-137	1.052(3)	0.030(2)	92
1274 keV, Eu-154/ 662 keV, Cs-137	1.161(3)	0.025(2)	93
1596 keV, Eu-154/ 662 keV, Cs-137	1.490(8)	0.078(6)	93
605 keV, Cs-134/ 662 keV, Cs-137	1.074(4)	0.026(3)	39
796 keV, Cs-134/ 662 keV, Cs-137	1.002(1)	0.007(1)	56
1365 keV, Cs-134/ 662 keV, Cs-137	1.248(5)	0.033(3)	46

which depend on the energy has not be taken into account. It can be a difference in the detector efficiency for instance or an attenuation plate that was overestimated/underestimated for one of the campaigns. For Table 5, the mean is closer to 1, but note that the attenuation plate properties (for stainless steel) were selected to give good agreements since the exact properties were unknown, in particular for the stainless steel (see Section 3.2). Hence it cannot be determined if systematic effects are also present in this measurement comparison. Fig. 8 shows the evolution of the weighted mean depending on the energy. It also shows a trend that depends on the energy, which is in adequation with unexact knowledge on the attenuation plates.

Tables 6 and 7 present the weighted mean values and weighted standard deviations of the net peak count for the selected peaks over the net peak count in the 662 keV peak from Cs-137 from campaign 1 over the same quantities in campaign 2. Tables 6 and 7 therefore, present the same results as Tables 4 and 5, except that the results are divided, corner by corner, by the respective Cs-137 net peak counts. This is done so that an easier comparison can be performed in Section 4.3, where only ratios are obtained.

4.2. Deviation in the net peak counts due to positioning of the fuel

At the Clab facility, the positioning of the SNF is fixed by the set-up. However, the distance between individual fuel rods and the detector can vary slightly, especially if the SNF has experienced any bowing. Moreover, the rotation angle of the SNF with respect to the detector is realized with a rotor moving step-wise and can potentially account for a high angular uncertainty with the current configuration of the set-up.

In order to estimate the net peak count uncertainty due to the positioning of the SNF and the detector, dedicated simulations are performed using the Feign code (Elter et al., 2019), an open-source Python package designed to compute the geometric efficiency for gamma measurements. The first set of simulations is performed to assess the impact of the positioning (distance) of the SNF with respect to the detector, and the results are presented in Fig. 9. The results show an increase/decrease in the count rate of 10% if the SNF is moved by 1 cm. This large effect is due to the fact that the attenuation of gamma rays in water is increased/decreased with a longer/shorter distance. Simulations are also done where only the detector is moved relative to the SNF (Fig. 9). As the detector is placed in air and sees a collimated gamma beam, the results show that the effect on the geometric efficiency is negligible (0.7%) as the gamma-ray attenuation in air is very low.

Finally, simulations are performed to investigate the impact of the rotation of the SNF with respect to the detector. The results show that by modifying the angle such that the detector is not facing exactly the corner of the SNF, the geometric efficiency is affected as the distance between the closest fuel pin and the detector is changed. For 10 degrees deviation, the attenuation is increased by 3%, as seen in Fig. 10. All these effects combined may explain the standard deviation (2.6% for BWR SNFs and 4.0% for the PWR SNFs) observed between the campaigns for Cs-137.

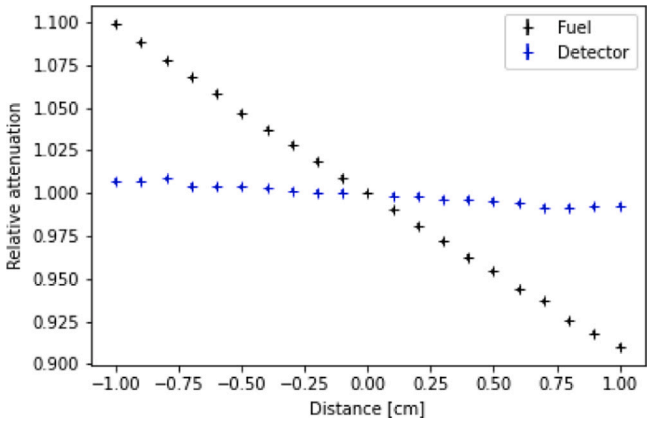

Fig. 9. Simulated relative attenuation depending on the SNF and detector position.

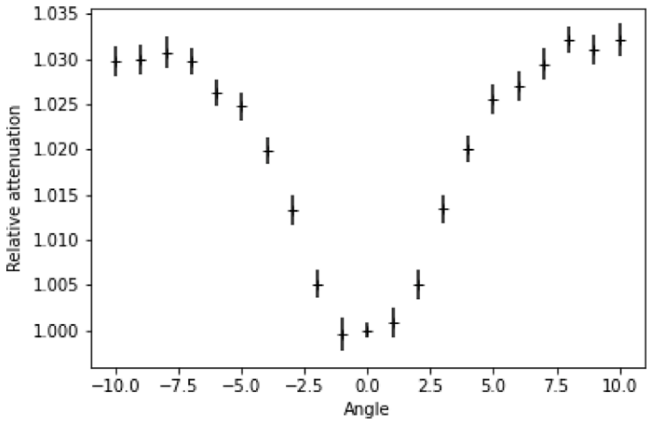

Fig. 10. Simulated relative attenuation depending on the angle SNF relative to the collimator opening.

The effect of positioning and rotation is however not dominant for Eu-154 and Cs-134, as the uncertainty on the net peak count themselves and reported in Tables C.15 and C.16 are dominant. Moreover, when considering the ratio between Cs-134 and Eu-154 over Cs-137, the effects cancel out or are negligible, except for the SNF position, where the attenuation in water acts differently on low- and high-energy gamma-rays. In this case the difference in attenuation for the most extreme energy separation with 662 keV (at 1596 keV) is 4% for a 1 cm deviation. Therefore, when determining the nuclides activities, in Section 4.3, one should preferably use the ratio of energy peaks close to each other to minimize this effect in the case where the position of SNF is not well-known, but this has not been further explored in this work as the position of the SNF is considered to be known in the current configuration.

4.3. Comparison with intrinsic self-calibration method

The polynomial fit of degree 2, explained in Section 3.3, needs to be calculated for each configuration of the system. In other words, if the geometry, detector, set-up, or attenuation plates changes, then the polynomial needs to be recalculated. In this work, four polynomials have been determined, one for each SNF type (BWR or PWR) and for each of the two campaigns. In campaign 1, as the attenuation plates are not well-known, no correction for them has been used before using the intrinsic self-calibration method. This is also used to demonstrate the capability of the intrinsic self-calibration method. For campaign 2, different sets of attenuation plates were used within the campaign. So either a different polynomial determination is needed for each configuration, or only one polynomial fit is needed if the net peak counts are corrected for the attenuation plates. The latter solution has been chosen as the attenuation plates in this campaign are well-known. The intrinsic self-calibration fit will still account for the other attenuations due to the water, detector efficiency, etc.

Table 8
Weighted mean and standard deviation of the ratio of relative activity for the ratio campaign 1 and campaign 2 for BWR assemblies. Nb is the number of measurements (corner × SNF) taken into account in the ratio.

BWR	Mean	Std	Nb
996 keV, Eu-154/ 662 keV, Cs-137	0.960(7)	0.051(5)	61
1004 keV, Eu-154/ 662 keV, Cs-137	0.972(4)	0.030(3)	64
1274 keV, Eu-154/ 662 keV, Cs-137	0.973(3)	0.025(2)	69
1596 keV, Eu-154/ 662 keV, Cs-137	1.020(8)	0.066(6)	62
605 keV, Cs-134/ 662 keV, Cs-137	1.144(21)	0.082(15)	16
796 keV, Cs-134/ 662 keV, Cs-137	0.971(3)	0.018(2)	27
1365 keV, Cs-134/ 662 keV, Cs-137	0.996(8)	0.043(6)	27

After performing the intrinsic self-calibration method, the relative activities in Tables 8 and 9 are calculated. A comparison with Tables 6 and 7 comprising the ratios of the net peak counts (without applying the intrinsic self-calibration) is performed. One can observe that the standard deviations for the ratios of relative activities are similar to the net peak counts ratios. This is an expected result since the two quantities are related to each other through the intrinsic self-calibration polynomial determined for all assemblies of the same type and campaign. The weighted mean of the ratios of the BWR SNFs is closer to 1.0 for the relative activities. For instance, the Eu-154 ratios between the two campaigns, the highest mean deviation from 1.0 reported in Table 8 is 4.0% (excluding the 1596 keV peak). For the Cs-134 the highest mean deviation is 2.9% (excluding the 605 keV peak). The 1596 keV peak and 605 keV peaks are excluded (but reported) because they are the highest and lowest energies considered, and therefore are associated with the highest uncertainty in the intrinsic self-calibration polynomial fit (p_{tot}). For the PWR case, the resulting ratios are even closer to 1.0 when compared with the results previously presented in Table 7. The highest deviation from 1.0 reported in Table 9 for the Eu-154 ratios is 1.7% compared to 16% (excluding the 1596 keV peak). For the Cs-134 ratios, it is 1.4% compared to 25%. Notice that the attenuation plates were not completely known in Table 7, which may introduce systematic errors and therefore explain the poorer performance in the case of PWR. When using the intrinsic self-calibration method, this lack of knowledge is not an issue; hence the agreement between campaigns is improved.

The complete list of Cs-137 count rates from campaign 2 can be found in the appendix in Tables D.18 and D.19 together with the Eu-154/Cs-137 and Cs-134/Cs-137 ratios after the intrinsic self-calibration. The ratios of Eu-154 in Tables D.18 and D.19 are calculated using the weighted average of the energy peaks at 996, 1004 and 1274 keV over the 662 keV peak from Cs-137. The ratio of Cs-134 over Cs-137 is calculated using the energy peaks at 796 keV and 1365 keV. The energy peak at 1596 keV is excluded since it is the most extreme energy; due to the deviations between campaigns 1 and 2, and due to relatively high systematic uncertainty (see Section 4.4), as well as having a significantly lower branching ratio. The peak at 605 keV is the lowest energy peak and is excluded for the same reason as the peak at 1596 keV.

Table 9
Weighted mean and standard deviation of the ratio of relative activity for the ratio campaign 1 and campaign 2 for PWR assemblies. *Nb* is the number of measurements (corner × SNF) taken into account in the ratio.

PWR	Mean	Std	Nb
996 keV, Eu-154/ 662 keV, Cs-137	0.983(4)	0.041(3)	85
1004 keV, Eu-154/ 662 keV, Cs-137	1.004(3)	0.028(2)	92
1274 keV, Eu-154/ 662 keV, Cs-137	0.985(2)	0.020(1)	93
1596 keV, Eu-154/ 662 keV, Cs-137	1.056(5)	0.053(4)	93
605 keV, Cs-134/ 662 keV, Cs-137	0.999(4)	0.023(3)	39
796 keV, Cs-134/ 662 keV, Cs-137	1.006(1)	0.008(1)	56
1365 keV, Cs-134/ 662 keV, Cs-137	1.014(4)	0.026(3)	46

4.4. Uncertainty investigation

Tables 10 and 11 present the random and systematic uncertainty calculated for each campaign and the ratio of campaigns using the methodology detailed in Section 3.4. Upon inspection of Tables 10 and 11, the systematic error in the relative activities has increased from campaign 1 to campaign 2 for both BWR and PWR SNFs. It is because time has passed between the two campaigns (2 years for the PWRs, and 5 years for the BWRs), which has an impact on the detectability of the short-lived radionuclides and thus on the uncertainty of the net peak count in the 605 keV peak since Cs-134 has a half-life of 2.1 years. Indeed most of the uncertainty actually comes from the determination of the attenuation in the Cs-137 peak from the intrinsic self-calibration fits. This peak is at low energy (662 keV), and there is only one peak at lower energy which is 605 keV. The 605 keV data point has great importance for the polynomial fit at low energies. The random uncertainty associated with this 605 kev point will translate through the intrinsic self-calibration polynomial to high systematic uncertainty in the low-energy region, in particular for the Cs-137 energy peak at 662 keV.

In Tables 10 and 11 the random uncertainty should be similar to the weighted standard deviation in Tables 8 and 9. In the appendix Tables B.13 and B.14, the two columns to compare are placed side to side. This confirms that the uncertainty calculated with the intrinsic self-calibration can explain the observed standard deviation. The systematic uncertainty in Tables 10 and 11 should also be similar to the mean deviations in Tables 8 and 9. However, it can be observed that the systematic uncertainty seems to be underestimated and cannot explain the mean deviation, especially for PWR SNFs. It can be partially explained by statistics, or by unknown causes. This does not represent more than 1.5%, and the trend does not depend on the energy or on the radionuclide.

Noted that the random uncertainty in Tables 10 and 11 is a weighted average, whereas the systematic uncertainty is a constant that only depends on the energy of the fit.

5. Discussion

To investigate the reproducibility of radionuclide activity determination, data from the measurement campaigns 1 and 2 have been evaluated. The peak areas were determined with a numerical integration. The results showed that the standard deviation associated with the peak count rate for the 662 keV peak from Cs-137 was 2% for the BWR SNFs and 4% for the PWR SNFs (see Tables 4 and 5). The analysis showed that the standard deviations cannot be explained by the uncertainty in the net peak area determination alone. Investigations related to the relative positioning of the SNF and detector was carried out for the Cs-137 peak. Up to 3% deviation in the attenuation is noted for a 10-degree rotation. Larger deviations (10% for 1 cm) can also be observed when the SNF's position is changed. The uncertainty of the placement and rotation within and between measurement campaigns is however not known, but it is reasonable to assume a small deviation is happening in reality. It cannot be excluded that the spread between the campaigns can be explained by the uncertainty in positioning. From this work, an uncertainty of 4% on the gamma activity needs to be assumed.

Ratios of net peak counts from Eu-154 and Cs-134 over the 662 keV peak from Cs-137 are also calculated for campaigns 1 and 2. The results from the 605 keV and 1596 keV peaks have been discarded since they are the most extreme energies and thus contain large uncertainties. The results show a small bias (average change between the campaigns) in the BWR cases where the attenuation is well-known, but a significant bias is found for the PWRs where the attenuation is not well-known. The PWR bias is, however, reduced when intrinsic self-calibration is employed.

After the intrinsic self-calibration, the bias ranges from 0.4–4.0% for the BWR SNFs and from 0.4–1.7% for the PWR SNFs (see Tables 8 and 9). This should be compared to the systematic uncertainty presented in Tables 10 and 11. The systematic uncertainty reported is underestimated as reported in Section 4.4 for PWR SNFs. An added systematic uncertainty of 1.5% should be assumed. The standard deviation in the inter-campaign reproducibility for the best-determined gamma peaks is then between 1 and 2%.

When irradiated in the reactor core, fuel assemblies are irradiated unevenly, creating differences in burnup between the different measured corners. Because of this, this work has been comparing SNF measurements corner by corner. It can be noted that on average, a standard deviation on the corners of the same assembly is around 4%. This effect is even more important for SNF with low BU and can reach more than 10% for BWR24 and BWR25.

6. Conclusion

A reference set of SNFs, the SKB-50 set, has been investigated with passive gamma spectroscopy in two measurement campaigns at the Clab facility. Campaign 1 was performed in 2014 and used an axial scan. Campaign 2 was performed in 2016 and 2019, also using axial scans and including a calibration Cs-137 source. The data from campaign 1 is made public with this work. Raw data from campaign 2 have been previously published, but this work includes an updated analysis of this data. The data is also made available in a computer-readable format for the first time.

In this work, a new algorithm that identifies when the SNF is in front of the detector has been developed. One gamma-ray spectrum is created for each corner measurement of each SNF. Net peaks counts for eight energy peaks for Eu-154, Cs-134 and Cs-137 are derived after having corrected for the use of attenuation plates placed between the SNF and the detector. Tables with the net peak count for campaigns 1 and 2 are in the appendix with uncertainties between 0.5 and 2%, which can be used for other studies. A sensitivity study on the positioning of the SNFs with respect to the detector shows that a deviation of 4% can be expected. A better control of the angle facing toward the detector for instance, would strongly reduce the uncertainty on the Cs-137 net peak counts.

In order to account for changes in attenuation and the energy dependence of the efficiency of the detector, an intrinsic self-calibration algorithm was developed. The methodology determines the relative activities of the different gamma peaks after correcting for the branching ratio, the attenuation, and the detector efficiency. The intrinsic self-attenuation reduces the required knowledge of the details of the measurement station. In this study, the bias from the attenuation plates unknowns for the PWR cases is reduced with the method. Particular emphasis is put on deriving and describing the uncertainty due to

Table 10
The uncertainty of the ratio of relative activity to Cs-137 for campaign 1, campaign 2 and the uncertainty of the ratio (of the above-mentioned ratio) of campaign 2 over campaign 1. Results for the BWR SKB-50 assemblies. The averaged random and systematic uncertainty depending on the energy peak for BWR assemblies calculated using equations presented in Section 3.4. The results presented are in percentage.

BWR	Campaign 1		Campaign 2		Ratio of campaigns	
	Random	Systematic	Random	Systematic	Random	Systematic
996 keV, Eu-154	4.9	0.4	7.9	2.5	6.6	2.5
1004 keV, Eu-154	3.1	0.4	5.4	2.5	4.2	2.5
1274 keV, Eu-154	1.2	0.3	1.9	2.4	1.4	2.4
1596 keV, Eu-154	4.5	0.4	6.5	2.5	5.5	2.5
605 keV, Cs-134	1.5	0.6	14.5	4.6	13.4	4.6
796 keV, Cs-134	0.6	0.4	2.8	2.6	2.2	2.6
1365 keV, Cs-134	1.8	0.3	6.1	2.4	4.9	2.5

Table 11
The uncertainty of the ratio of relative activity to Cs-137 for campaign 1, campaign 2 and the uncertainty of the ratio (of the above-mentioned ratio) of campaign 2 over campaign 1. Results for the PWR SKB-50 assemblies. The averaged random and systematic uncertainty depending on the energy peak for PWR assemblies calculated using equations presented in Section 3.4. The results presented are in percentage.

PWR	Campaign 1		Campaign 2		Ratio of campaigns	
	Random	Systematic	Random	Systematic	Random	Systematic
996 keV, Eu-154	4.6	0.2	4.9	0.4	5.0	0.4
1004 keV, Eu-154	2.9	0.2	3.4	0.4	3.3	0.4
1274 keV, Eu-154	1.0	0.2	1.1	0.3	1.1	0.4
1596 keV, Eu-154	3.7	0.2	5.4	0.4	5.3	0.4
605 keV, Cs-134	1.6	0.3	3.2	0.5	1.5	0.6
796 keV, Cs-134	3.9	0.2	6.8	0.4	0.6	0.5
1365 keV, Cs-134	3.9	0.2	9.2	0.3	1.5	0.4

intrinsic self-calibration. The intrinsic self-calibration is easy to apply, it only required to have one or several SNFs with short-cooling time, in order to determine the attenuation curve. It can then be applied to longer cooled SNFs.

The final results on the net peak count for Cs-137, and the ratio of Eu-154 and Cs-134 over Cs-137 after the intrinsic self-calibration is presented (see Appendix D), for all SKB-50 SNFs measured during campaign 2.

It is shown that both methods show that the net peak counts and relative activities in the selected peaks are reproducible quantities (within two sigmas) over the different campaigns within uncertainties originating in e.g. SNF positioning, detector set-up, etc. But using an intrinsic self-calibration methodology allows for reducing the bias in the results and does not require extensive knowledge of the set-up.

In this work, for both measurement campaigns, the HPGe detectors have been used. In the future, different kinds of detectors could be used. To use the intrinsic self-calibration with a different detector, it requires to use a high-resolution detector, which is able to measure different well-separated full-energy peaks at different energy ranges, in particular for Eu-154 and Cs-134.

Table A.12
Different corners measured for the different campaigns. 1 indicates that this corner or this SNF has been measured in campaign 1. 2 indicates that this corner or this SNF has been measured in campaign 2.

Angle	45°	135°	225°	315°	Angle	45°	135°	225°	315°
BWR01	1	1	1	1	PWR01	1, 2	1, 2	1, 2	1, 2
BWR02	1, 2	1, 2	1, 2	1, 2	PWR02	1, 2	1, 2	1, 2	1, 2
BWR03	1, 2	1, 2	1, 2	1, 2	PWR03	1	1	1	1
BWR04	1	1	1	1	PWR04	1, 2	1, 2	1, 2	1, 2
BWR05	1, 2	1, 2	1, 2	2	PWR05	1, 2	1, 2	1, 2	1, 2
BWR06	1, 2	1, 2	1, 2	1, 2	PWR06	1	1	1	1
BWR07	1, 2	1, 2	1, 2	1, 2	PWR07	1, 2	1, 2	1, 2	1, 2
BWR08	1	1	1	1	PWR08	1	1, 2	1, 2	1, 2
BWR09	1	1	1	1	PWR09	1, 2	1, 2	1, 2	1, 2
BWR10	1, 2	1, 2	1, 2	1	PWR10	1, 2	1	1, 2	1
BWR11	1, 2	1, 2	1, 2	1	PWR11	1	1, 2	1	1, 2
BWR12	1, 2	1, 2	1, 2	1	PWR12	1, 2	1, 2	1, 2	1, 2
BWR13	1, 2	2	1	1, 2	PWR13	1, 2	1, 2	1, 2	1, 2
BWR14	1, 2	1, 2	1, 2	1, 2	PWR14	1, 2	1, 2	1, 2	1, 2
BWR15	1, 2	1, 2	1, 2	1, 2	PWR15	1, 2	1, 2	1, 2	1, 2
BWR16	1, 2	1, 2	1, 2	1, 2	PWR16	1, 2	1	1, 2	1, 2
BWR17	1	1, 2	1, 2	1, 2	PWR17	1	1, 2	1, 2	1, 2
BWR18	1, 2	1, 2	1, 2	1, 2	PWR18	1, 2	1, 2	1, 2	1, 2
BWR19	1, 2	1, 2	1, 2	1, 2	PWR19	1, 2	1, 2	1, 2	1, 2
BWR20	1	1	1	1	PWR20	1	1, 2	1, 2	1, 2
BWR21	1, 2	1, 2	1, 2	1, 2	PWR21	1, 2	1, 2	1	2
BWR22	1, 2	1, 2	1, 2	1, 2	PWR22	1, 2	1	1, 2	1, 2
BWR23	1	1	1	1	PWR23	1, 2	1, 2	1, 2	1, 2
BWR24	1, 2	1, 2	1, 2	1, 2	PWR24	1, 2	1, 2	1, 2	1, 2
BWR25	1, 2	1, 2	1, 2	1, 2	PWR25	1, 2	2	1, 2	1, 2

Table B.13
Results for the BWR SKB-50 assemblies. The (weighted mean-1)/weighted mean and standard deviation of the ratio of relative activity over Cs-137 for the ratio of campaign 2 over campaign 1. The averaged random and systematic uncertainty depending on the energy peak for BWR assemblies calculated using equations presented in Section 3.4. The results presented are in percentages.

BWR	Mean	Systematic	Std	Random
996 keV, Eu-154	−4.2	2.5	5.2	6.6
1004 keV, Eu-154	−3.0	2.5	2.9	4.2
1274 keV, Eu-154	−3.2	2.4	2.1	1.4
1596 keV, Eu-154	1.6	2.5	6.1	5.5
605 keV, Cs-134	12.4	4.6	7.1	13.4
796 keV, Cs-134	−3.2	2.6	1.7	2.2
1365 keV, Cs-134	−0.4	2.5	4.1	4.9

Table B.14
Results for the PWR SKB-50 assemblies. The (weighted mean - 1)/weighted mean and standard deviation of the ratio of relative activity over Cs-137 for the ratio of campaign 2 over campaign 1. The averaged random and systematic uncertainty depending on the energy peak for PWR assemblies calculated using equations presented in Section 3.4. The results presented are in percentages.

PWR	Mean	Systematic	Std	Random
996 keV, Eu-154	−1.7	0.4	4.2	5.0
1004 keV, Eu-154	0.4	0.4	2.8	3.3
1274 keV, Eu-154	−1.4	0.4	2.1	1.1
1596 keV, Eu-154	5.3	0.4	5.0	5.3
605 keV, Cs-134	−0.2	0.6	2.3	1.5
796 keV, Cs-134	0.6	0.5	0.7	0.6
1365 keV, Cs-134	1.5	0.4	2.5	1.5

CRediT authorship contribution statement

Virginie Solans: Methodology, Software, Formal analysis, Writing – original draft, Writing – review & editing. **Henrik Sjöstrand:** Writing – review & editing, Supervision. **Peter Jansson:** Conceptualization, Resources, Writing – review & editing, Supervision. **Peter Schillebeeckx:** Methodology, Writing – review & editing, Supervision. **Sophie Grape:** Writing – review & editing, Supervision. **Erik Branger:** Writing – review & editing, Supervision. **Anders Sjöland:** Writing – review & editing, Supervision, Funding acquisition.

Declaration of competing interest

The authors declare the following financial interests/personal relationships which may be considered as potential competing interests: Virginie Solans reports financial support was provided by EURAD.

Data availability

I have shared the data in the appendix. A computer version can also be shared.

Acknowledgment

The project leading to this publication has received funding from the European Union's Horizon 2020 research and innovation program under grant agreement No 847593.

Appendix A. Measurement corners for the different campaigns

See Table A.12.

Appendix B. Compare mean, std and random and systematic uncertainties

See Tables B.13 and B.14.

Appendix C. Net peak

See Tables C.15–C.17.

Appendix D. Relative activities

See Tables D.18 and D.19.

Table C.15
Net peak measured for some peaks from Cs-137, Eu-154 and Cs-134. For the campaign 1 done in 2014. Not corrected for the attenuation plates.

SNF	Corner	Cs-137 662 keV (cps)	Unc. (%)	Eu-154 996 keV (cps)	Unc. (%)	Eu-154 1004 keV (cps)	Unc. (%)	Eu-154 1274 keV (cps)	Unc. (%)	Eu-154 1596 keV (cps)	Unc. (%)	Cs-134 605 keV (cps)	Unc. (%)	Cs-134 796 keV (cps)	Unc. (%)	Cs-134 1365 keV (cps)	Unc. (%)
BWR10	45	3175.82	0.14	32.06	2.77	57.9	1.68	173.87	0.6	12.6	2.47	309.75	0.92	572.22	0.36	58.49	1.08
BWR10	135	3193.96	0.14	34.44	2.65	59.11	1.68	178.46	0.6	12.43	2.59	321.95	0.91	589.4	0.36	60.63	1.06
BWR10	225	3090.57	0.14	32.93	2.72	56.69	1.74	170.62	0.61	12.05	2.55	303.4	0.94	560.09	0.37	57.7	1.11
BWR10	315	3080.98	0.14	32.14	3.52	55.78	1.73	170.58	0.61	11.86	2.66	296.53	0.95	544.89	0.37	57.48	1.09
BWR11	45	1347.99	0.17	6.15	4.67	10.62	3.02	32.97	1.11	2.41	4.34	0.0	nan	2.4	14.84	0.0	nan
BWR11	135	1435.74	0.16	7.18	4.23	11.84	2.81	36.86	1.02	2.56	4.14	0.0	nan	2.66	13.67	0.0	nan
BWR11	225	1406.97	0.17	6.88	4.54	11.81	2.9	36.63	1.07	2.5	4.39	0.0	nan	0.0	nan	0.0	nan
BWR11	315	1226.02	0.17	5.38	4.99	9.63	3.05	28.64	1.14	2.19	4.42	0.0	nan	1.9	16.88	0.0	nan
BWR12	45	2473.03	0.14	24.57	2.63	42.31	1.68	130.11	0.61	8.93	2.52	136.9	1.52	255.87	0.52	26.22	1.49
BWR12	135	2465.33	0.14	23.19	2.8	42.77	1.64	127.67	0.62	8.84	2.57	139.29	1.49	258.93	0.51	26.83	1.45
BWR12	225	2370.05	0.14	22.71	2.7	40.01	1.66	121.5	0.62	8.43	2.62	129.44	1.53	238.61	0.52	24.23	1.5
BWR12	315	2464.96	0.14	24.48	2.69	42.25	1.72	128.79	0.63	9.12	2.47	136.1	1.55	249.96	0.53	25.9	1.52
BWR13	45	2658.21	0.14	25.43	2.81	45.75	1.71	143.57	0.61	10.21	2.52	154.55	1.48	289.94	0.5	30.69	1.42
BWR13	225	2774.57	0.14	26.84	2.77	48.87	1.66	148.42	0.6	10.05	3.31	172.58	1.36	319.98	0.48	32.38	1.4
BWR13	315	2749.09	0.14	28.19	2.58	48.86	1.63	146.52	0.61	10.48	2.46	163.69	1.4	296.58	0.5	30.85	1.43
BWR14	45	1231.89	0.18	3.42	7.23	6.85	3.91	20.18	1.46	1.46	5.87	0.0	nan	0.0	nan	0.0	nan
BWR14	135	1164.04	0.18	3.43	6.79	6.33	4.01	19.35	1.42	1.33	6.98	0.0	nan	0.0	nan	0.0	nan
BWR14	225	1182.77	0.18	3.6	6.62	6.36	4.09	20.29	1.38	1.33	6.04	0.0	nan	0.0	nan	0.0	nan
BWR14	315	1261.64	0.18	4.35	11.19	7.15	3.85	21.78	1.37	1.57	5.32	0.0	nan	0.0	nan	0.0	nan
BWR15	45	1200.47	0.18	4.32	5.82	7.7	3.55	22.96	1.33	1.64	5.35	0.0	nan	0.0	nan	0.0	nan
BWR15	135	1193.26	0.17	4.25	5.77	7.4	4.88	22.93	1.29	1.67	4.97	0.0	nan	0.0	nan	0.0	nan
BWR15	225	1188.92	0.17	4.3	5.54	7.76	3.8	23.13	1.27	1.65	4.99	0.0	nan	0.0	nan	0.0	nan
BWR15	315	1146.38	0.17	3.81	7.74	7.21	3.61	21.6	1.3	1.6	5.15	0.0	nan	0.0	nan	0.0	nan
BWR16	45	1110.04	0.18	3.78	6.02	6.7	3.79	20.5	1.36	1.35	5.94	0.0	nan	0.0	nan	0.0	nan
BWR16	135	1156.39	0.18	4.01	5.68	6.91	3.67	20.45	1.39	1.4	5.52	0.0	nan	0.0	nan	0.0	nan
BWR16	225	1086.96	0.18	3.78	5.77	6.34	6.59	19.27	1.38	1.36	5.7	0.0	nan	0.0	nan	0.0	nan
BWR16	315	1044.88	0.18	3.82	5.77	6.51	3.64	19.68	1.37	1.33	5.84	0.0	nan	0.0	nan	0.0	nan
BWR17	45	1234.02	0.17	4.52	5.36	7.81	3.43	24.11	1.23	1.72	4.72	0.0	nan	0.0	nan	0.0	nan
BWR17	135	1323.76	0.17	4.95	5.45	8.38	3.45	25.12	1.28	1.78	4.88	0.0	nan	0.0	nan	0.0	nan
BWR17	225	1275.97	0.17	4.81	6.58	8.59	3.25	25.3	1.26	1.84	5.09	0.0	nan	0.0	nan	0.0	nan
BWR17	315	1201.64	0.17	4.64	5.16	7.84	3.42	24.02	1.24	1.67	4.93	0.0	nan	0.0	nan	0.0	nan
BWR18	45	930.35	0.19	3.77	5.94	6.89	3.52	20.83	1.3	1.3	5.92	0.0	nan	1.6	16.94	0.0	nan
BWR18	135	1010.92	0.19	4.5	5.44	7.73	3.48	23.67	1.28	1.57	5.43	0.0	nan	0.0	nan	0.0	nan
BWR18	225	963.28	0.2	4.0	7.38	6.76	3.88	20.66	1.41	1.36	5.9	0.0	nan	1.57	18.61	0.0	nan
BWR18	315	896.58	0.2	3.48	7.57	5.73	4.07	18.45	1.41	1.22	6.12	0.0	nan	0.0	nan	0.0	nan
BWR19	45	1332.83	0.17	5.45	4.99	9.22	3.24	29.14	1.15	2.01	4.76	0.0	nan	0.0	nan	0.0	nan
BWR19	135	1341.6	0.17	5.33	5.22	9.12	3.27	27.99	1.2	2.05	4.67	0.0	nan	0.0	nan	0.0	nan
BWR19	225	1343.04	0.17	4.94	8.02	9.06	3.23	28.62	1.15	2.01	4.58	0.0	nan	0.0	nan	0.0	nan
BWR19	315	1338.22	0.17	5.79	4.57	9.69	3.1	28.01	1.18	2.02	4.52	0.0	nan	0.0	nan	0.0	nan
BWR01	45	3465.01	0.13	33.41	2.66	58.31	1.66	176.43	0.59	12.7	2.41	253.86	1.11	474.02	0.4	48.68	1.19
BWR01	135	3569.06	0.13	32.52	2.85	59.81	1.67	179.85	0.6	12.82	2.48	274.13	1.07	504.9	0.4	51.66	1.19
BWR01	225	3631.77	0.13	33.82	2.76	60.07	1.68	178.6	0.61	12.54	2.61	271.79	1.09	496.86	0.41	50.73	1.22
BWR01	315	3519.56	0.13	32.27	2.83	59.04	1.66	176.39	0.6	12.09	2.66	249.15	1.15	467.78	0.41	48.35	1.22

(*continued on next page*)

Table C.15 (*continued*).

SNF	Corner	Cs-137 662 keV (cps)	Unc. (%)	Eu-154 996 keV (cps)	Unc. (%)	Eu-154 1004 keV (cps)	Unc. (%)	Eu-154 1274 keV (cps)	Unc. (%)	Eu-154 1596 keV (cps)	Unc. (%)	Cs-134 605 keV (cps)	Unc. (%)	Cs-134 796 keV (cps)	Unc. (%)	Cs-134 1365 keV (cps)	Unc. (%)
BWR20	45	1944.83	0.15	17.05	3.01	29.97	1.87	89.4	0.71	6.32	2.77	104.34	1.67	193.2	0.56	19.83	1.61
BWR20	135	2041.78	0.16	18.39	3.06	31.46	1.93	96.57	0.71	7.02	2.66	118.83	1.58	215.74	0.55	21.78	1.61
BWR20	225	2016.2	0.15	18.31	2.93	31.58	1.86	94.09	0.7	6.46	3.06	111.12	1.64	204.1	0.55	20.43	1.61
BWR20	315	1959.2	0.15	16.3	3.25	29.11	1.98	91.18	0.71	6.33	2.85	102.57	1.73	189.13	0.57	20.26	1.6
BWR21	45	999.34	0.19	3.59	12.09	6.07	4.85	19.5	1.38	1.36	5.55	0.0	nan	0.0	nan	0.0	nan
BWR21	135	1041.78	0.18	3.8	5.77	6.32	3.9	19.31	1.38	1.25	7.07	0.0	nan	0.0	nan	0.0	nan
BWR21	225	1042.28	0.18	3.53	6.21	6.55	3.55	19.44	1.36	1.32	5.51	0.0	nan	0.0	nan	0.0	nan
BWR21	315	1012.89	0.18	3.68	5.93	5.99	4.03	19.29	1.36	1.39	5.56	0.0	nan	0.0	nan	0.0	nan
BWR22	45	1499.66	0.17	9.74	5.02	16.96	2.48	51.63	0.92	3.66	3.65	54.18	2.64	99.32	0.78	10.21	2.2
BWR22	135	1568.89	0.17	10.3	4.04	18.57	2.43	56.69	0.88	3.74	3.6	63.35	2.37	114.69	0.73	11.64	2.12
BWR22	225	1605.35	0.17	10.61	4.01	19.41	2.38	57.59	0.9	4.05	3.38	64.47	2.4	120.95	0.72	12.0	2.1
BWR22	315	1531.56	0.17	9.95	4.09	17.42	2.59	53.17	0.93	3.65	3.75	54.84	2.72	105.83	0.77	10.94	2.25
BWR23	45	1070.25	0.18	5.44	9.21	9.25	3.19	28.89	1.13	2.09	4.41	31.61	3.44	58.83	0.94	6.04	2.73
BWR23	135	1193.27	0.18	6.4	6.2	11.18	3.05	34.12	1.11	2.26	4.64	39.74	3.09	72.14	0.89	7.51	2.53
BWR23	225	1264.21	0.18	6.6	4.82	12.21	2.83	35.9	1.07	2.55	8.93	44.02	2.87	80.31	0.83	7.98	2.37
BWR23	315	1201.44	0.18	6.38	4.71	11.45	2.9	32.73	1.1	2.46	4.14	39.3	3.07	70.5	0.88	7.25	2.48
BWR24	45	535.77	0.25	1.43	10.03	2.28	15.33	7.07	3.25	0.0	nan	0.0	nan	0.0	nan	0.0	nan
BWR24	135	451.04	0.27	1.19	12.19	2.0	8.0	6.04	2.52	0.36	14.24	0.0	nan	0.0	nan	0.0	nan
BWR24	225	496.85	0.25	1.18	14.35	2.0	7.76	6.64	2.34	0.46	10.6	0.0	nan	0.0	nan	0.0	nan
BWR24	315	580.33	0.24	1.41	11.66	2.53	6.43	7.57	2.23	0.56	9.54	0.0	nan	0.0	nan	0.0	nan
BWR25	45	336.24	0.31	0.61	16.89	1.0	14.85	3.22	3.46	0.0	nan	0.0	nan	0.0	nan	0.0	nan
BWR25	135	259.53	0.35	0.5	18.54	0.74	13.91	2.69	3.68	0.0	nan	0.0	nan	0.0	nan	0.0	nan
BWR25	225	309.74	0.32	0.0	nan	0.83	14.09	2.85	3.66	0.2	19.79	0.0	nan	0.0	nan	0.0	nan
BWR25	315	402.05	0.29	0.66	15.76	1.07	12.53	3.54	3.48	0.0	nan	0.0	nan	0.0	nan	0.0	nan
BWR02	45	3218.08	0.13	28.12	4.68	50.78	1.69	154.55	0.61	11.02	2.61	154.54	1.62	287.84	0.53	29.54	1.55
BWR02	135	3227.79	0.13	26.78	2.91	48.06	1.75	146.99	0.62	10.82	2.48	150.35	1.64	278.38	0.53	28.36	1.59
BWR02	225	3230.41	0.13	27.65	2.85	47.99	1.78	147.22	0.63	10.7	2.57	156.17	1.61	287.67	0.53	29.97	1.53
BWR02	315	3185.12	0.13	29.31	2.62	51.05	1.66	153.24	0.6	11.1	2.4	156.37	1.57	291.19	0.52	29.11	1.54
BWR03	45	2976.91	0.13	23.54	2.8	40.94	1.76	127.01	0.64	8.8	2.56	69.57	3.11	126.59	0.87	13.01	2.43
BWR03	135	3157.07	0.13	24.73	2.74	44.59	1.64	132.36	0.62	9.41	2.51	75.5	2.89	141.27	0.79	14.57	2.55
BWR03	225	3225.04	0.13	24.19	2.85	44.78	1.69	133.81	0.63	9.19	2.76	71.05	3.18	135.85	0.84	14.07	2.39
BWR03	315	3054.05	0.13	23.38	2.9	41.17	1.78	125.31	0.66	8.75	2.82	67.42	3.31	125.07	0.9	13.0	2.52
BWR04	45	2860.27	0.13	22.81	3.69	39.71	1.71	121.58	0.63	8.64	2.46	56.63	3.6	108.62	0.93	11.17	2.59
BWR04	135	2728.45	0.13	21.63	2.84	38.38	1.74	115.69	0.65	8.07	2.65	52.92	3.8	103.17	0.95	11.07	2.63
BWR04	225	2853.8	0.13	22.27	2.83	40.61	1.67	122.09	0.62	8.8	2.49	61.74	3.27	114.47	0.88	11.66	2.53
BWR04	315	3106.99	0.13	25.01	3.37	42.93	1.72	132.5	0.62	9.41	2.47	67.09	3.27	124.05	0.89	12.81	2.49
BWR04	0	3247.98	0.81	27.35	16.23	52.09	8.76	142.15	3.89	0.0	nan	0.0	nan	142.33	5.1	0.0	nan
BWR05	45	3135.38	0.13	28.84	2.76	50.31	1.74	154.07	0.61	11.12	2.48	235.84	1.09	432.26	0.4	44.58	1.19
BWR05	135	3377.65	0.13	33.33	2.61	57.06	1.65	171.05	0.6	12.05	2.5	261.81	1.06	483.37	0.39	48.27	1.19
BWR05	225	3226.3	0.13	30.38	2.71	53.93	1.67	160.18	0.61	11.29	2.51	236.33	1.12	433.21	0.41	44.26	1.23
BWR06	45	1561.91	0.16	4.96	6.12	9.82	3.36	29.31	1.22	2.07	4.94	0.0	nan	0.0	nan	0.0	nan
BWR06	135	1478.36	0.16	4.97	7.29	8.52	3.57	26.47	1.26	1.81	5.32	0.0	nan	0.0	nan	0.0	nan
BWR06	225	1502.84	0.16	5.01	5.75	8.65	3.74	27.97	1.22	2.04	5.09	0.0	nan	0.0	nan	0.0	nan
BWR06	315	1554.12	0.16	5.63	5.36	9.75	3.37	30.61	1.16	2.12	4.71	0.0	nan	0.0	nan	0.0	nan
BWR07	45	2980.64	0.13	26.2	2.69	45.13	1.73	136.89	0.63	10.11	2.4	128.49	1.78	235.4	0.57	24.98	1.62
BWR07	135	3192.15	0.13	27.11	2.79	47.8	1.74	144.75	0.62	10.01	2.62	143.72	1.69	261.0	0.56	26.75	1.6
BWR07	225	3035.18	0.13	26.11	2.81	46.99	1.68	141.78	0.62	10.23	2.43	134.68	1.74	249.63	0.56	26.13	1.58
BWR07	315	2831.37	0.14	24.18	6.83	43.34	1.78	134.72	0.63	9.13	2.62	121.53	1.84	227.19	0.58	23.93	1.63
BWR08	45	2911.67	0.14	29.42	6.28	51.42	1.65	158.42	0.59	11.04	2.45	214.62	1.14	396.52	0.42	40.86	1.23
BWR08	135	2832.93	0.14	28.42	2.75	49.52	1.72	153.67	0.61	11.08	2.44	202.42	1.21	384.75	0.43	40.31	1.24
BWR08	225	2806.37	0.14	27.66	2.8	49.67	1.67	153.88	0.59	11.25	2.4	197.8	1.22	378.39	0.43	39.46	1.24
BWR08	315	2959.78	0.14	30.66	2.65	52.92	1.66	162.23	0.6	11.43	2.47	216.61	1.17	401.32	0.43	42.94	1.23
BWR09	45	3224.82	0.14	31.68	2.84	55.88	1.74	170.0	0.61	11.9	2.65	346.71	0.83	634.02	0.34	64.22	1.01
BWR09	135	3372.39	0.14	32.86	2.89	58.62	1.73	177.69	0.61	12.28	2.7	374.59	0.81	679.08	0.33	69.0	1.0
BWR09	225	3158.37	0.14	31.22	4.07	53.73	1.81	162.1	0.64	11.4	2.79	321.25	0.9	592.51	0.36	61.34	1.06
BWR09	315	3038.93	0.14	29.6	2.85	51.7	1.79	158.29	0.62	11.54	2.63	297.18	0.93	554.85	0.36	57.67	1.06
PWR10	45	1050.69	0.19	11.31	3.26	21.15	1.93	73.25	0.69	6.04	2.48	7.75	13.36	18.34	2.6	3.02	5.02
PWR10	135	1192.69	0.18	13.09	3.06	23.65	1.84	84.19	0.65	6.69	2.45	8.54	13.15	22.8	2.28	3.41	4.78
PWR10	225	1184.76	0.18	13.1	3.01	23.64	1.86	85.58	0.65	6.78	2.3	9.01	12.33	22.5	2.33	3.49	4.57
PWR10	315	1073.83	0.19	12.18	3.16	21.88	1.92	76.97	0.69	6.44	2.37	7.45	14.35	18.04	2.77	2.99	5.22
PWR11	45	1038.58	0.19	12.14	3.22	22.46	1.89	81.47	0.66	6.54	2.46	9.1	11.52	22.46	2.26	3.6	4.62
PWR11	135	1158.0	0.18	15.09	2.72	26.19	1.72	92.56	0.61	7.28	2.25	12.17	9.01	29.92	1.85	4.32	4.19
PWR11	225	1144.81	0.18	14.33	2.87	25.69	1.77	90.48	0.62	7.47	2.34	11.0	15.75	27.25	1.99	4.14	4.31
PWR11	315	1005.88	0.19	12.35	3.02	21.03	1.96	76.74	0.67	6.18	2.33	0.0	nan	19.69	2.45	2.95	5.63
PWR12	45	905.23	0.2	5.48	6.28	10.4	3.34	35.98	1.02	2.84	4.16	0.0	nan	0.0	nan	0.0	nan
PWR12	135	871.67	0.21	5.56	6.05	9.62	3.54	34.96	1.03	2.85	3.73	0.0	nan	0.0	nan	0.0	nan
PWR12	225	910.89	0.2	6.17	7.9	10.22	3.34	35.71	1.04	2.93	3.73	0.0	nan	0.0	nan	0.0	nan
PWR12	315	949.69	0.2	6.22	5.59	10.81	3.25	37.22	1.01	3.04	3.78	0.0	nan	0.0	nan	0.0	nan
PWR13	315	781.29	0.22	4.26	5.73	7.74	3.42	27.28	1.15	2.1	4.98	0.0	nan	0.0	nan	0.0	nan
PWR13	45	722.75	0.22	4.03	5.55	7.29	3.41	25.45	1.18	2.09	4.3	0.0	nan	0.0	nan	0.0	nan
PWR13	135	756.17	0.22	4.23	5.59	7.61	3.32	26.76	1.14	2.15	4.22	0.0	nan	0.0	nan	0.0	nan
PWR13	225	801.65	0.21	4.3	5.67	7.72	3.41	28.34	1.13	2.14	4.34	0.0	nan	0.0	nan	0.0	nan

(*continued on next page*)

Table C.15 (*continued*).

SNF	Corner	Cs-137 662 keV (cps)	Unc. (%)	Eu-154 996 keV (cps)	Unc. (%)	Eu-154 1004 keV (cps)	Unc. (%)	Eu-154 1274 keV (cps)	Unc. (%)	Eu-154 1596 keV (cps)	Unc. (%)	Cs-134 605 keV (cps)	Unc. (%)	Cs-134 796 keV (cps)	Unc. (%)	Cs-134 1365 keV (cps)	Unc. (%)
PWR14	45	940.43	0.21	10.21	4.28	17.86	2.5	64.57	0.76	5.42	2.61	0.0	nan	12.12	6.64	1.96	10.46
PWR14	135	907.83	0.2	0.0	nan	16.33	2.57	60.1	0.75	4.7	2.93	0.0	nan	10.67	19.94	1.76	10.73
PWR14	225	1078.0	0.19	11.73	4.02	20.99	2.26	73.54	0.72	5.87	2.57	0.0	nan	14.75	3.87	2.15	7.57
PWR14	315	1076.37	0.19	11.94	3.9	20.97	2.28	73.83	0.71	6.09	2.59	0.0	nan	15.15	3.8	2.34	9.4
PWR15	315	818.11	0.21	5.02	4.97	8.65	3.2	31.38	1.05	2.44	3.9	0.0	nan	0.0	nan	0.0	nan
PWR15	45	802.04	0.21	4.85	5.16	8.89	3.07	30.24	1.09	2.44	5.92	0.0	nan	0.0	nan	0.0	nan
PWR15	135	761.52	0.21	4.4	5.38	8.6	2.98	28.88	1.09	2.27	4.06	0.0	nan	0.0	nan	0.0	nan
PWR15	225	802.02	0.21	4.81	10.48	8.45	3.16	30.47	1.04	2.31	3.95	0.0	nan	0.0	nan	0.0	nan
PWR16	45	962.14	0.2	9.46	5.45	15.89	2.59	59.01	0.76	4.75	2.75	0.0	nan	8.04	5.97	1.14	18.89
PWR16	135	973.94	0.19	9.85	4.19	17.12	2.44	59.72	0.77	4.76	2.77	0.0	nan	8.25	5.84	1.36	10.59
PWR16	225	1008.65	0.2	10.51	4.09	17.85	2.47	63.57	0.76	4.84	2.85	0.0	nan	9.29	5.5	1.44	10.21
PWR16	315	961.12	0.2	9.18	4.49	16.2	2.53	58.16	0.78	4.76	2.97	0.0	nan	7.64	6.25	1.46	8.88
PWR17	45	1060.99	0.2	12.93	5.04	23.26	2.22	82.62	0.68	6.69	2.52	10.17	13.32	27.5	2.37	4.7	4.13
PWR17	135	981.1	0.2	11.87	3.91	20.97	2.25	76.29	0.68	6.2	2.41	9.58	12.98	25.54	2.33	4.08	5.18
PWR17	225	1024.81	0.2	13.14	3.63	22.08	2.22	79.06	0.67	6.18	2.52	0.0	nan	27.21	2.29	4.21	4.41
PWR17	315	1092.22	0.19	14.15	3.56	24.28	2.11	85.41	0.66	6.92	2.37	11.32	11.82	29.48	2.22	4.39	4.37
PWR18	315	866.83	0.21	7.59	5.21	14.39	2.3	49.99	0.83	3.87	3.03	0.0	nan	4.0	8.81	0.69	15.52
PWR18	45	836.75	0.21	7.82	3.81	13.65	2.38	48.85	0.84	3.74	3.13	0.0	nan	3.77	9.39	0.81	12.94
PWR18	135	896.56	0.2	8.0	3.81	13.78	2.41	50.74	0.82	4.13	2.91	0.0	nan	3.59	10.37	0.63	16.82
PWR18	225	930.02	0.2	8.42	4.61	14.4	2.4	52.01	0.82	4.09	2.96	0.0	nan	4.38	8.29	0.72	15.02
PWR19	45	593.28	0.24	2.48	8.01	4.97	4.31	17.07	1.48	1.32	5.8	0.0	nan	0.0	nan	0.0	nan
PWR19	135	648.75	0.23	3.13	9.37	5.36	4.07	19.21	1.35	1.46	5.54	0.0	nan	0.0	nan	0.0	nan
PWR19	225	665.64	0.23	3.08	6.57	5.67	3.95	20.17	1.31	1.53	5.14	0.0	nan	0.0	nan	0.0	nan
PWR19	315	583.71	0.24	2.73	7.19	4.75	4.25	17.03	1.42	1.42	5.64	0.0	nan	0.0	nan	0.0	nan
PWR01	315	1811.46	0.19	41.24	2.51	72.32	1.56	261.45	0.47	20.36	2.18	512.13	0.54	1265.22	0.22	191.14	0.53
PWR01	45	1845.59	0.2	40.85	2.67	75.7	1.55	266.72	0.49	19.81	2.36	519.53	0.55	1286.85	0.22	194.73	0.55
PWR01	135	1708.47	0.19	37.43	2.62	69.14	1.53	243.28	0.48	18.44	2.31	458.5	0.56	1141.74	0.23	176.13	0.54
PWR01	225	1735.32	0.2	39.67	2.63	71.3	1.59	254.81	0.49	19.49	2.3	476.02	0.58	1187.35	0.23	182.73	0.56
PWR20	45	677.75	0.23	3.65	18.75	6.38	4.39	22.68	1.32	1.98	4.57	0.0	nan	0.0	nan	0.0	nan
PWR20	135	665.81	0.24	3.66	7.49	6.64	4.14	22.07	1.3	1.79	4.83	0.0	nan	0.0	nan	0.0	nan
PWR20	225	659.28	0.23	3.42	7.88	5.74	5.29	21.24	1.34	1.74	4.76	0.0	nan	0.0	nan	0.0	nan
PWR20	315	653.08	0.23	3.41	7.8	6.3	4.14	21.48	1.31	1.63	5.18	0.0	nan	0.0	nan	0.0	nan
PWR21	45	649.85	0.24	3.62	7.46	6.25	4.37	21.61	1.34	1.69	4.93	0.0	nan	0.0	nan	0.0	nan
PWR21	135	671.22	0.23	0.0	nan	6.08	4.6	22.12	1.31	1.83	5.02	0.0	nan	0.0	nan	0.0	nan
PWR21	225	659.15	0.23	3.44	8.11	6.32	4.36	21.88	1.33	0.0	nan	0.0	nan	0.0	nan	0.0	nan
PWR22	45	624.85	0.24	3.6	7.07	0.0	nan	20.26	1.36	1.73	5.0	0.0	nan	0.0	nan	0.0	nan
PWR22	135	581.39	0.25	3.01	10.94	5.1	4.99	18.59	1.41	1.59	5.16	0.0	nan	0.0	nan	0.0	nan
PWR22	225	577.75	0.25	3.32	7.49	5.12	5.0	18.11	1.44	1.47	5.67	0.0	nan	0.0	nan	0.0	nan
PWR22	315	629.35	0.24	3.73	6.92	5.74	5.44	20.73	1.38	1.69	4.89	0.0	nan	0.0	nan	0.0	nan
PWR23	45	647.93	0.24	5.3	6.06	9.66	3.37	34.35	1.03	2.68	4.54	0.0	nan	5.79	6.46	0.95	11.79
PWR23	135	692.73	0.23	5.8	5.66	9.99	3.31	35.39	1.01	2.86	3.52	0.0	nan	5.76	6.77	0.95	12.28
PWR23	225	720.65	0.22	5.81	5.73	10.35	3.23	37.06	0.99	3.05	3.56	0.0	nan	5.96	11.7	0.0	nan
PWR23	315	648.6	0.23	5.31	6.05	9.81	3.22	33.54	1.01	2.79	3.69	0.0	nan	5.7	6.48	1.0	10.33
PWR24	45	420.01	0.29	0.0	nan	5.94	3.76	21.98	1.24	1.65	4.93	0.0	nan	0.0	nan	0.0	nan
PWR24	135	423.31	0.29	3.36	5.95	5.96	3.73	21.3	1.27	1.65	4.86	0.0	nan	1.25	18.79	0.0	nan
PWR24	225	462.45	0.28	4.01	5.49	6.72	3.54	24.21	1.17	1.84	4.78	0.0	nan	1.53	16.33	0.0	nan
PWR24	315	441.48	0.28	3.76	10.78	7.15	3.2	24.28	1.16	1.91	4.22	0.0	nan	0.0	nan	0.0	nan
PWR25	45	364.46	0.31	0.0	nan	2.31	9.62	8.69	2.05	0.53	10.77	0.0	nan	0.0	nan	0.0	nan
PWR25	225	349.25	0.31	1.16	13.49	2.4	6.79	8.28	2.05	0.59	9.67	0.0	nan	0.0	nan	0.0	nan
PWR25	315	349.91	0.31	1.32	10.59	2.17	7.79	8.28	2.04	0.61	8.92	0.0	nan	0.0	nan	0.0	nan
PWR02	315	1626.94	0.19	36.7	2.43	64.44	1.5	225.75	0.48	17.87	2.08	368.39	0.64	915.14	0.25	141.56	0.59
PWR02	45	1693.6	0.19	37.91	2.49	65.74	1.56	238.0	0.48	18.47	2.14	431.1	0.58	1057.03	0.23	159.51	0.56
PWR02	135	1708.67	0.2	39.25	2.5	67.81	1.58	243.07	0.48	19.11	2.17	455.14	0.57	1107.13	0.23	166.73	0.56
PWR02	225	1631.92	0.19	35.46	2.57	63.56	1.56	230.12	0.48	17.88	2.18	388.41	0.62	971.78	0.24	148.78	0.58
PWR03	45	1204.51	0.18	15.56	3.93	28.3	1.69	101.56	0.59	8.22	2.42	18.55	6.19	46.39	1.35	7.1	2.78
PWR03	135	1246.52	0.18	15.75	2.85	29.07	1.68	103.97	0.59	8.27	2.22	19.95	10.15	49.74	1.29	7.76	3.0
PWR03	225	1400.47	0.17	17.8	2.71	32.84	1.62	115.25	0.57	8.91	3.15	23.74	5.39	57.22	1.23	8.42	2.67
PWR03	315	1338.95	0.17	17.94	2.55	31.61	1.6	110.71	0.57	8.69	2.09	22.17	5.45	54.47	1.22	8.38	2.56
PWR04	45	1487.26	0.19	32.43	3.02	57.25	1.5	202.08	0.49	15.74	2.05	262.83	0.78	657.96	0.29	100.24	0.69
PWR04	135	1520.22	0.19	32.24	2.43	57.58	1.49	205.08	0.48	15.9	1.99	276.17	0.74	684.65	0.28	104.41	0.67
PWR04	225	1520.91	0.19	33.41	3.13	56.66	1.48	202.01	0.48	15.8	1.94	253.1	0.79	636.14	0.29	97.97	0.69
PWR04	315	1481.6	0.19	31.06	2.4	53.72	1.52	196.35	0.49	15.08	2.03	241.29	0.81	604.63	0.3	93.31	0.7
PWR05	45	1482.03	0.19	30.8	2.46	55.38	1.47	194.51	0.49	15.51	1.98	248.12	0.8	618.61	0.3	95.66	0.69
PWR05	135	1487.6	0.19	31.7	3.76	55.43	1.53	196.34	0.5	15.2	2.04	247.04	0.82	615.21	0.3	93.81	0.71
PWR05	225	1527.01	0.19	31.49	2.45	57.49	1.47	201.62	0.48	15.97	1.98	269.06	0.76	665.69	0.28	100.97	0.67
PWR05	315	1584.15	0.19	33.62	2.44	58.21	1.54	209.68	0.49	16.56	2.02	289.88	0.75	714.12	0.28	106.44	0.68
PWR06	315	1142.49	0.18	14.11	2.9	25.09	1.8	89.6	0.63	7.04	2.58	12.25	11.42	32.19	1.73	4.96	3.63
PWR06	45	1149.98	0.19	14.28	2.88	25.59	1.79	92.1	0.63	7.32	2.3	12.87	8.68	32.64	1.73	5.2	3.43
PWR06	135	1181.21	0.18	14.77	2.76	26.51	1.71	93.69	0.61	7.47	6.08	12.92	8.5	31.13	1.78	4.67	3.73
PWR06	225	1202.3	0.18	15.47	2.71	26.7	1.72	94.72	0.61	7.29	2.22	11.96	12.17	31.49	1.78	4.95	3.8
PWR06	0	1327.31	1.28	0.0	nan	30.01	11.23	89.81	5.14	0.0	nan	0.0	nan	40.17	10.31	0.0	nan
PWR07	45	1383.87	0.19	28.58	2.34	48.58	1.51	176.68	0.49	13.93	1.94	174.95	1.0	436.16	0.35	66.36	0.82

(*continued on next page*)

Table C.15 (*continued*).

SNF	Corner	Cs-137 662 keV (cps)	Unc. (%)	Eu-154 996 keV (cps)	Unc. (%)	Eu-154 1004 keV (cps)	Unc. (%)	Eu-154 1274 keV (cps)	Unc. (%)	Eu-154 1596 keV (cps)	Unc. (%)	Cs-134 605 keV (cps)	Unc. (%)	Cs-134 796 keV (cps)	Unc. (%)	Cs-134 1365 keV (cps)	Unc. (%)
PWR07	135	1438.33	0.19	28.86	2.4	51.01	1.5	179.87	0.5	14.19	1.89	188.5	0.97	466.08	0.34	71.0	0.8
PWR07	225	1373.37	0.19	25.92	2.59	46.97	1.54	169.27	0.51	13.23	2.01	163.16	1.06	408.6	0.37	62.82	0.84
PWR07	315	1318.47	0.19	24.86	2.5	45.1	1.5	161.82	0.5	12.46	1.98	152.43	1.07	378.14	0.37	58.91	0.84
PWR08	45	879.29	0.2	5.6	4.72	10.39	2.79	36.83	0.96	3.01	3.51	0.0	nan	0.0	nan	0.0	nan
PWR08	135	907.85	0.2	6.03	4.81	10.4	2.92	38.17	0.96	3.03	3.71	0.0	nan	0.0	nan	0.0	nan
PWR08	225	915.27	0.2	6.21	4.33	10.92	2.73	37.84	0.96	3.0	3.61	0.0	nan	0.0	nan	0.0	nan
PWR08	315	902.17	0.2	5.95	4.62	10.38	2.86	37.14	0.97	2.92	3.9	0.0	nan	0.0	nan	0.0	nan
PWR09	315	1464.42	0.18	28.48	2.38	50.69	1.48	178.34	0.49	14.43	1.9	189.57	0.95	473.74	0.33	71.69	0.78
PWR09	45	1392.83	0.18	27.57	2.32	47.02	1.51	168.77	0.5	13.39	1.94	163.16	1.04	412.51	0.35	64.11	0.81
PWR09	135	1458.74	0.18	28.56	2.37	50.97	1.47	179.36	0.49	13.67	2.15	187.24	0.96	465.57	0.34	71.44	0.78
PWR09	225	1537.1	0.18	28.86	2.51	53.02	1.48	187.7	0.49	14.5	2.0	215.05	0.89	530.92	0.32	80.26	0.75

Table C.16
Net peak measured for some peaks from Cs-137, Eu-154 and Cs-134. For the campaign 2 done in 2016–2019. Corrected for the attenuation plates.

SNF	Corner	Cs-137 662 keV (cps)	Unc. (%)	Eu-154 996 keV (cps)	Unc. (%)	Eu-154 1004 keV (cps)	Unc. (%)	Eu-154 1274 keV (cps)	Unc. (%)	Eu-154 1596 keV (cps)	Unc. (%)	Cs-134 605 keV (cps)	Unc. (%)	Cs-134 796 keV (cps)	Unc. (%)	Cs-134 1365 keV (cps)	Unc. (%)
BWR02	45	2938.1	0.21	19.28	3.98	33.64	2.76	100.34	0.87	7.05	3.45	41.41	14.83	63.74	2.46	6.75	8.59
BWR02	135	2917.39	0.2	18.08	3.98	31.74	2.74	94.08	0.87	6.53	3.64	41.68	17.61	60.14	2.48	6.21	6.09
BWR02	225	2922.74	0.2	17.2	4.22	32.13	2.72	95.1	0.87	6.98	3.42	45.54	12.98	63.97	2.37	6.23	5.21
BWR02	315	2930.67	0.21	18.02	4.2	34.76	2.65	98.62	0.87	7.17	3.44	46.47	16.9	65.78	2.38	6.21	5.43
BWR03	45	2752.0	0.21	15.06	4.5	27.08	3.02	81.37	0.96	6.24	3.7	0.0	nan	28.87	4.62	3.12	9.12
BWR03	135	2963.73	0.2	15.9	4.43	29.82	2.89	88.47	0.91	6.42	3.65	0.0	nan	33.03	4.16	3.25	8.89
BWR03	225	2936.72	0.2	16.36	4.11	29.24	2.74	83.98	0.91	6.21	3.55	0.0	nan	31.49	4.14	3.11	9.23
BWR03	315	2738.83	0.2	14.82	4.39	26.47	2.95	78.38	0.94	5.78	3.66	0.0	nan	27.25	4.6	2.88	9.1
BWR05	45	2907.28	0.21	20.67	3.68	34.49	2.7	103.23	0.85	7.57	3.29	57.92	13.66	100.72	1.65	9.79	3.8
BWR05	135	3104.04	0.2	21.64	14.48	36.56	2.67	111.68	0.83	7.66	3.59	71.68	8.95	107.91	1.64	10.89	3.6
BWR05	225	2966.09	0.2	20.3	3.71	35.05	2.58	104.51	0.83	7.34	3.38	68.66	12.35	96.16	1.7	9.81	3.68
BWR05	315	2765.0	0.21	18.44	3.86	31.63	2.73	96.21	0.85	7.11	3.86	58.42	9.85	91.52	1.69	9.49	3.65
BWR06	45	1430.93	0.27	3.4	10.02	6.64	6.18	18.78	1.98	1.54	7.59	0.0	nan	0.0	nan	0.0	nan
BWR06	135	1404.62	0.28	3.37	10.32	6.02	9.76	18.24	2.02	1.35	8.58	0.0	nan	0.0	nan	0.0	nan
BWR06	225	1418.08	0.27	3.52	11.88	6.44	8.29	18.82	1.96	1.28	8.35	0.0	nan	0.0	nan	0.0	nan
BWR06	315	1451.84	0.26	3.81	9.15	6.52	6.38	18.95	1.97	1.52	7.46	0.0	nan	0.0	nan	0.0	nan
BWR07	45	2750.8	0.21	17.06	4.25	29.12	3.0	87.85	0.93	6.19	3.82	0.0	nan	52.71	2.81	5.85	5.64
BWR07	225	2766.62	0.21	17.09	4.11	31.45	2.71	90.38	0.88	6.37	3.68	0.0	nan	55.5	2.59	5.4	5.74
BWR07	315	2570.99	0.21	16.1	4.17	27.44	2.94	85.27	0.9	6.45	3.61	33.76	16.07	50.13	2.72	5.29	5.5
BWR07	135	2888.7	0.2	17.53	4.04	30.11	2.82	92.25	0.86	6.53	3.48	44.49	16.62	57.36	2.5	6.32	4.87
BWR10	45	2870.16	0.21	21.99	3.51	37.86	2.46	109.7	0.81	7.79	3.24	0.0	nan	126.92	1.37	12.77	3.01
BWR10	135	2893.41	0.21	20.58	3.85	37.79	2.52	111.08	0.8	8.03	3.26	82.21	10.41	128.91	1.37	12.99	3.0
BWR10	225	2785.83	0.21	20.33	3.7	35.95	2.53	108.21	0.8	7.84	3.16	77.68	14.44	121.53	1.39	12.62	2.96
BWR11	45	1204.44	0.29	3.51	11.86	6.96	5.87	20.42	1.82	1.6	7.17	0.0	nan	0.0	nan	0.0	nan
BWR11	135	1319.18	0.28	4.69	7.42	8.02	5.3	23.54	1.67	1.89	6.27	0.0	nan	0.0	nan	0.0	nan
BWR11	225	1268.67	0.29	4.28	8.36	7.75	5.56	23.57	1.71	1.5	7.9	0.0	nan	0.0	nan	0.0	nan
BWR12	45	2268.72	0.22	14.94	4.38	27.96	2.81	82.79	0.9	6.04	3.58	40.53	19.21	58.01	2.33	5.68	5.12
BWR12	135	2228.39	0.22	15.28	4.15	26.92	2.81	81.63	0.89	5.7	3.58	40.1	16.02	58.3	2.25	5.51	5.09
BWR12	225	2245.73	0.23	15.35	4.28	27.73	2.85	83.08	0.92	5.7	3.94	39.78	16.93	57.84	2.39	5.66	5.16
BWR13	45	2409.2	0.22	16.76	3.96	30.73	2.62	87.93	0.88	6.53	3.41	0.0	nan	63.11	2.22	6.02	5.07
BWR13	135	2408.02	0.22	18.08	7.91	29.43	2.73	88.1	0.87	6.37	3.48	0.0	nan	65.6	2.15	6.72	4.54
BWR13	315	2457.67	0.21	17.32	3.97	30.45	2.71	92.84	0.84	6.62	3.33	43.04	12.23	65.75	2.14	6.25	4.83
BWR14	45	1152.73	0.3	2.91	10.43	4.67	7.82	14.26	2.3	1.18	9.01	0.0	nan	0.0	nan	0.0	nan
BWR14	135	1130.93	0.3	2.49	14.58	4.37	10.39	13.07	2.39	1.1	9.09	0.0	nan	0.0	nan	0.0	nan
BWR14	225	1136.68	0.3	2.21	13.08	4.48	7.79	13.59	2.36	1.09	9.06	0.0	nan	0.0	nan	0.0	nan
BWR14	315	1166.05	0.29	2.85	10.45	4.83	7.32	14.25	2.23	0.91	10.44	0.0	nan	0.0	nan	0.0	nan
BWR15	45	1104.59	0.3	2.7	10.82	5.41	6.54	14.5	2.18	1.22	8.25	0.0	nan	0.0	nan	0.0	nan
BWR15	135	1113.38	0.29	3.1	9.25	5.13	6.74	15.77	2.04	1.04	8.84	0.0	nan	0.0	nan	0.0	nan
BWR15	225	1157.36	0.3	3.22	9.56	5.21	8.19	16.51	2.09	1.29	8.34	0.0	nan	0.0	nan	0.0	nan
BWR15	315	1144.07	0.3	3.28	9.14	4.9	7.32	16.12	2.12	1.23	8.17	0.0	nan	0.0	nan	0.0	nan
BWR16	45	994.91	0.31	2.33	15.05	4.32	7.52	12.59	2.33	0.0	nan	0.0	nan	0.0	nan	0.0	nan
BWR16	135	1068.56	0.3	2.96	9.31	5.0	7.56	13.31	2.31	1.05	9.47	0.0	nan	0.0	nan	0.0	nan
BWR16	225	1028.58	0.31	2.66	10.31	4.7	7.23	13.29	2.3	0.93	10.0	0.0	nan	0.0	nan	0.0	nan
BWR16	315	960.07	0.31	2.32	11.5	4.07	7.82	12.96	2.25	1.06	8.99	0.0	nan	0.0	nan	0.0	nan
BWR17	135	1212.02	0.29	3.14	9.88	5.69	6.61	17.22	2.04	1.3	8.28	0.0	nan	0.0	nan	0.0	nan
BWR17	225	1159.43	0.29	3.06	9.86	5.62	6.5	15.73	2.09	1.2	9.32	0.0	nan	0.0	nan	0.0	nan
BWR17	315	1124.41	0.3	2.81	15.3	5.42	6.97	15.92	2.09	1.26	8.29	0.0	nan	0.0	nan	0.0	nan
BWR18	45	897.35	0.34	2.96	12.75	4.6	7.72	14.09	2.29	1.02	9.79	0.0	nan	0.0	nan	0.0	nan
BWR18	135	917.07	0.33	2.8	13.25	5.36	6.51	15.22	2.12	0.97	11.14	0.0	nan	0.0	nan	0.0	nan
BWR18	225	850.51	0.34	2.51	14.15	4.79	6.62	12.49	2.35	0.96	9.81	0.0	nan	0.0	nan	0.0	nan
BWR18	315	831.01	0.35	2.19	12.46	4.25	7.64	12.5	2.35	0.9	10.2	0.0	nan	0.0	nan	0.0	nan
BWR19	45	1226.38	0.29	3.42	19.3	5.96	6.57	18.84	1.9	1.48	7.45	0.0	nan	0.0	nan	0.0	nan
BWR19	135	1208.16	0.28	3.54	8.88	6.17	6.08	18.39	1.92	1.48	7.15	0.0	nan	0.0	nan	0.0	nan

(*continued on next page*)

Table C.16 (*continued*).

SNF	Corner	Cs-137 662 keV (cps)	Unc. (%)	Eu-154 996 keV (cps)	Unc. (%)	Eu-154 1004 keV (cps)	Unc. (%)	Eu-154 1274 keV (cps)	Unc. (%)	Eu-154 1596 keV (cps)	Unc. (%)	Cs-134 605 keV (cps)	Unc. (%)	Cs-134 796 keV (cps)	Unc. (%)	Cs-134 1365 keV (cps)	Unc. (%)
BWR19	225	1259.69	0.28	3.62	11.16	6.2	6.32	18.75	1.94	1.44	7.73	0.0	nan	0.0	nan	0.0	nan
BWR19	315	1252.78	0.28	3.75	8.64	6.59	6.07	19.03	1.91	1.61	7.04	0.0	nan	0.0	nan	0.0	nan
BWR21	45	911.46	0.32	2.12	12.57	4.22	7.54	12.77	2.28	0.9	9.69	0.0	nan	0.0	nan	0.0	nan
BWR21	135	975.72	0.32	2.57	10.64	4.57	10.99	12.75	2.39	1.0	9.45	0.0	nan	0.0	nan	0.0	nan
BWR21	225	963.15	0.3	2.27	11.41	4.4	7.11	12.87	2.22	0.99	8.98	0.0	nan	0.0	nan	0.0	nan
BWR21	315	935.72	0.31	0.0	nan	3.95	8.15	13.51	2.2	0.92	10.2	0.0	nan	0.0	nan	0.0	nan
BWR22	45	1360.28	0.27	5.99	8.99	10.97	4.47	32.43	1.4	2.46	5.25	0.0	nan	21.77	3.92	2.3	8.35
BWR22	135	1446.52	0.28	7.24	6.2	13.14	4.12	37.23	1.37	2.79	5.6	20.92	19.04	27.1	3.44	2.53	8.21
BWR22	225	1449.08	0.27	7.01	6.16	12.61	4.16	36.27	1.36	2.82	5.16	0.0	nan	27.26	3.36	2.81	7.42
BWR22	315	1379.14	0.28	6.67	8.47	11.0	4.65	34.4	1.38	2.41	6.37	0.0	nan	23.79	3.68	2.54	7.79
BWR24	45	497.38	0.44	0.95	19.41	1.81	13.47	4.81	4.23	0.0	nan	0.0	nan	0.0	nan	0.0	nan
BWR24	135	397.39	0.47	0.0	nan	0.0	nan	3.75	4.73	0.41	15.99	0.0	nan	0.0	nan	0.0	nan
BWR24	225	488.33	0.45	0.0	nan	1.51	15.25	4.91	4.04	0.0	nan	0.0	nan	0.0	nan	0.0	nan
BWR24	315	528.48	0.41	0.0	nan	1.77	12.44	5.37	3.73	0.41	16.42	0.0	nan	0.0	nan	0.0	nan
BWR25	45	310.21	0.53	0.0	nan	0.0	nan	2.13	7.02	0.0	nan	0.0	nan	0.0	nan	0.0	nan
BWR25	135	237.75	0.62	0.0	nan	0.0	nan	1.74	7.97	0.0	nan	0.0	nan	0.0	nan	0.0	nan
BWR25	225	283.38	0.56	0.0	nan	0.0	nan	1.75	7.78	0.0	nan	0.0	nan	0.0	nan	0.0	nan
BWR25	315	347.75	0.5	0.0	nan	0.0	nan	2.44	6.07	0.0	nan	0.0	nan	0.0	nan	0.0	nan
PWR01	135	11 147.23	0.26	131.92	6.57	249.23	4.21	677.43	1.38	48.51	10.74	1946.76	1.64	3004.21	0.67	277.36	2.65
PWR01	225	11 080.29	0.24	121.68	6.46	234.73	4.04	678.43	1.25	50.53	9.16	1914.33	1.5	3009.34	0.6	279.92	2.36
PWR01	315	11 805.43	0.26	141.43	6.69	242.24	4.75	715.14	1.42	51.29	11.3	2090.5	1.62	3260.38	0.66	293.53	2.75
PWR01	45	11 364.66	0.15	128.52	3.07	240.59	1.98	709.75	0.61	52.13	3.76	1961.4	0.96	3171.02	0.32	298.49	1.04
PWR01	135	10 759.48	0.15	129.7	2.79	230.67	1.89	676.74	0.58	47.09	3.76	1791.19	0.98	2905.13	0.32	277.9	1.02
PWR01	225	10 709.15	0.15	130.18	2.72	234.65	1.83	681.53	0.58	48.34	3.62	1799.78	0.96	2938.12	0.31	275.5	1.02
PWR01	315	11 390.82	0.15	143.16	2.72	249.88	1.89	714.58	0.6	51.9	3.79	1983.51	0.94	3203.53	0.31	301.21	1.03
PWR01	45	10 926.47	0.15	133.38	2.21	242.23	1.47	704.33	0.46	50.96	2.42	1847.22	0.98	3041.47	0.28	290.18	0.76
PWR01	135	10 356.54	0.15	128.39	2.19	226.59	1.49	670.46	0.46	48.49	2.39	1681.38	1.03	2796.8	0.29	273.13	0.77
PWR01	225	10 335.08	0.15	126.51	2.2	228.58	1.47	674.78	0.46	49.11	2.36	1677.93	1.03	2827.62	0.28	277.2	0.76
PWR01	315	10 961.42	0.15	135.46	2.18	247.43	1.44	709.69	0.46	49.97	2.51	1873.91	0.98	3091.42	0.28	296.4	0.75
PWR02	45	11 117.77	0.25	127.64	6.4	233.38	4.26	650.07	1.34	49.33	9.65	1802.18	1.68	2791.89	0.67	255.5	2.66
PWR02	225	10 568.46	0.21	110.37	5.89	219.77	3.56	624.74	1.1	45.82	7.95	1584.54	1.53	2501.26	0.59	228.63	2.3
PWR02	315	10 522.25	0.21	118.99	5.24	221.53	3.4	625.27	1.08	42.91	8.18	1521.42	1.56	2378.01	0.6	219.03	2.33
PWR02	45	10 792.87	0.14	126.4	2.74	225.48	1.85	659.78	0.58	46.05	3.65	1687.73	1.0	2716.57	0.32	251.01	1.06
PWR02	135	10 803.37	0.14	131.28	2.68	236.18	1.81	665.94	0.58	49.07	3.5	1765.3	0.97	2814.06	0.32	258.89	1.06
PWR02	225	10 207.99	0.14	123.71	2.55	218.18	1.74	627.82	0.56	44.21	3.41	1502.44	1.04	2445.94	0.33	229.88	1.05
PWR02	315	10 245.15	0.14	118.5	2.65	214.04	1.77	619.88	0.56	45.08	3.31	1439.19	1.08	2343.49	0.34	219.98	1.08
PWR04	45	9651.52	0.19	0.0	nan	196.81	2.94	562.02	0.91	40.83	6.21	1128.04	1.66	1772.0	0.61	157.43	2.32
PWR04	135	9878.23	0.19	111.66	5.7	193.53	3.13	566.68	0.95	42.29	6.32	1191.68	1.65	1863.82	0.61	168.14	2.32
PWR04	225	9791.88	0.18	110.45	4.23	193.24	2.94	543.58	0.93	40.72	6.13	1069.8	1.73	1689.11	0.62	152.96	2.34
PWR04	315	9578.12	0.18	104.55	4.25	190.27	2.84	541.76	0.89	37.37	6.25	1033.93	1.72	1630.53	0.62	149.25	2.29
PWR05	45	9667.5	0.18	104.79	4.3	190.98	2.85	538.77	0.9	37.74	6.26	1022.33	1.76	1627.84	0.62	146.92	2.34
PWR05	135	9509.85	0.18	101.27	4.31	186.17	2.82	536.38	0.88	39.34	5.78	994.92	1.76	1573.96	0.63	145.1	2.28
PWR05	225	9733.44	0.19	103.89	4.63	198.34	2.93	551.96	0.94	43.05	5.92	1111.96	1.72	1735.88	0.63	157.28	2.37
PWR05	315	9960.73	0.19	110.47	4.52	190.7	3.16	559.1	0.96	43.11	6.15	1166.54	1.68	1800.84	0.63	164.26	2.34
PWR07	45	8936.53	0.17	95.55	3.82	171.72	2.59	486.07	0.82	35.19	5.18	749.91	2.03	1182.15	0.69	108.49	2.46
PWR07	135	9132.96	0.17	99.81	3.77	180.12	2.53	492.6	0.83	35.42	5.36	790.06	1.97	1241.54	0.68	112.27	2.47
PWR07	225	8667.06	0.16	90.49	3.65	162.21	2.48	456.51	0.79	32.62	5.01	683.86	2.04	1074.92	0.69	98.98	2.42
PWR07	315	8607.17	0.16	88.99	3.66	159.89	2.47	452.22	0.79	33.15	4.82	654.23	2.11	1038.53	0.7	96.54	2.43
PWR08	135	5798.51	0.12	19.69	5.63	36.62	3.65	102.61	1.12	7.64	5.35	0.0	nan	0.0	nan	0.0	nan
PWR08	225	5824.52	0.12	19.96	5.61	36.29	3.7	102.35	1.12	7.52	5.42	0.0	nan	0.0	nan	0.0	nan
PWR08	315	5718.71	0.12	20.63	5.21	36.35	3.54	103.16	1.08	7.26	5.44	0.0	nan	0.0	nan	0.0	nan
PWR09	135	9386.74	0.17	94.01	4.11	169.17	2.75	486.96	0.85	33.05	5.89	778.88	2.05	1212.71	0.71	111.73	2.52
PWR09	225	9931.82	0.17	104.14	4.11	187.95	2.74	522.06	0.89	36.65	5.99	882.21	1.98	1384.47	0.69	122.56	2.6
PWR09	315	9576.14	0.17	92.04	4.33	170.33	2.81	492.78	0.87	35.05	5.72	799.08	2.05	1239.49	0.71	113.98	2.54
PWR09	45	8792.96	0.13	88.49	2.44	160.55	1.61	472.72	0.51	32.86	2.79	655.83	1.73	1065.58	0.47	101.79	1.39
PWR09	135	9105.97	0.13	94.92	2.35	166.72	1.63	488.94	0.52	34.04	2.83	723.78	1.63	1180.04	0.45	111.61	1.35
PWR09	225	9671.22	0.13	102.02	2.42	182.17	1.63	520.39	0.53	37.69	2.85	843.86	1.51	1353.57	0.43	122.46	1.36
PWR09	315	9278.63	0.13	95.36	2.41	173.42	1.59	499.15	0.52	35.21	2.82	744.61	1.62	1225.26	0.44	113.93	1.35
PWR10	45	6762.52	0.13	41.14	3.71	70.95	2.61	206.97	0.8	14.71	4.2	0.0	nan	49.77	5.94	4.76	16.91
PWR10	225	7575.55	0.13	48.53	3.67	83.15	2.59	235.25	0.82	15.98	4.66	0.0	nan	59.77	5.8	5.61	17.08
PWR11	135	7296.59	0.12	50.94	3.37	88.24	2.35	254.11	0.74	17.78	4.07	54.41	15.53	80.35	4.12	7.93	14.66
PWR11	315	6341.51	0.12	40.55	3.44	73.2	2.31	209.05	0.74	14.54	3.98	0.0	nan	51.15	5.24	4.55	16.1
PWR12	45	5789.63	0.13	18.72	5.9	33.47	3.96	98.52	1.15	6.7	5.99	0.0	nan	0.0	nan	0.0	nan
PWR12	135	6033.36	0.12	20.29	5.61	37.31	4.21	101.57	1.16	7.04	6.17	0.0	nan	0.0	nan	0.0	nan
PWR12	225	5725.04	0.13	19.49	5.55	34.38	3.81	99.45	1.13	6.92	5.6	0.0	nan	0.0	nan	0.0	nan
PWR12	315	5455.39	0.12	18.31	5.56	34.05	3.55	93.03	1.12	6.93	5.35	0.0	nan	0.0	nan	0.0	nan
PWR13	45	5180.98	0.13	15.74	5.93	28.92	3.89	76.83	1.26	5.67	5.75	0.0	nan	0.0	nan	0.0	nan
PWR13	135	5036.2	0.13	15.05	6.01	25.72	4.24	75.7	1.23	5.4	6.05	0.0	nan	0.0	nan	0.0	nan
PWR13	225	4702.8	0.13	13.95	5.96	25.82	3.9	71.03	1.22	5.2	5.58	0.0	nan	0.0	nan	0.0	nan
PWR13	315	4843.63	0.13	14.8	5.74	26.82	3.84	72.17	1.23	5.5	5.44	0.0	nan	0.0	nan	0.0	nan
PWR14	45	5864.62	0.13	34.45	3.68	60.76	2.53	171.97	0.82	12.34	4.07	0.0	nan	31.68	7.72	0.0	nan
PWR14	135	6021.92	0.13	34.5	3.79	61.15	2.6	173.74	0.83	11.91	4.28	0.0	nan	29.91	8.44	0.0	nan

(*continued on next page*)

Table C.16 (*continued*).

SNF	Corner	Cs-137 662 keV (cps)	Unc. (%)	Eu-154 996 keV (cps)	Unc. (%)	Eu-154 1004 keV (cps)	Unc. (%)	Eu-154 1274 keV (cps)	Unc. (%)	Eu-154 1596 keV (cps)	Unc. (%)	Cs-134 605 keV (cps)	Unc. (%)	Cs-134 796 keV (cps)	Unc. (%)	Cs-134 1365 keV (cps)	Unc. (%)
PWR14	225	6775.04	0.13	39.65	3.86	70.9	2.61	201.51	0.83	14.84	4.07	0.0	nan	37.07	7.94	4.41	17.89
PWR14	315	6726.82	0.13	39.56	3.85	70.06	2.63	202.63	0.82	14.79	4.16	0.0	nan	40.65	7.29	4.21	18.75
PWR15	45	5496.14	0.13	18.31	5.57	31.62	3.9	92.4	1.14	6.35	5.83	0.0	nan	0.0	nan	0.0	nan
PWR15	135	5529.16	0.12	17.05	6.03	32.12	3.84	92.24	1.14	6.1	6.17	0.0	nan	0.0	nan	0.0	nan
PWR15	225	5092.48	0.13	16.55	5.65	29.77	3.8	84.1	1.17	5.9	5.74	0.0	nan	0.0	nan	0.0	nan
PWR15	315	5033.81	0.13	17.0	5.42	30.0	3.71	83.9	1.14	5.79	5.91	0.0	nan	0.0	nan	0.0	nan
PWR16	45	6325.64	0.13	32.97	4.09	59.95	2.72	167.96	0.87	11.42	4.57	0.0	nan	21.53	12.11	0.0	nan
PWR16	225	6282.64	0.12	34.35	3.86	59.04	2.74	168.97	0.85	11.96	4.38	0.0	nan	24.41	10.51	0.0	nan
PWR16	315	6111.13	0.13	32.34	3.99	57.13	2.74	162.98	0.86	11.61	4.38	0.0	nan	20.94	11.91	0.0	nan
PWR17	135	6173.92	0.12	38.89	3.52	71.37	2.31	204.99	0.73	14.64	3.72	39.79	17.77	67.45	3.91	6.29	11.25
PWR17	225	6520.16	0.12	42.64	3.42	76.27	2.31	216.87	0.74	15.4	3.91	45.41	16.52	68.8	4.14	6.72	11.43
PWR17	315	7371.71	0.16	47.39	4.69	86.2	3.1	242.74	0.98	16.59	5.49	0.0	nan	83.07	5.16	7.31	16.42
PWR18	45	5444.48	0.12	27.56	3.86	48.72	2.66	135.84	0.86	9.49	4.4	0.0	nan	11.11	18.4	0.0	nan
PWR18	135	5598.11	0.12	27.49	4.0	47.06	2.83	136.35	0.87	10.1	4.16	0.0	nan	0.0	nan	0.0	nan
PWR18	225	5879.05	0.12	28.35	4.2	49.69	2.89	140.56	0.91	10.33	4.47	0.0	nan	0.0	nan	0.0	nan
PWR18	315	5739.17	0.12	27.4	4.21	48.59	2.87	141.03	0.89	10.06	4.42	0.0	nan	0.0	nan	0.0	nan
PWR19	45	4325.27	0.13	12.03	6.13	20.86	4.29	56.06	1.35	4.04	6.19	0.0	nan	0.0	nan	0.0	nan
PWR19	135	3922.8	0.13	10.07	6.62	16.93	4.74	49.74	1.38	3.67	8.66	0.0	nan	0.0	nan	0.0	nan
PWR19	225	3825.06	0.13	9.45	8.69	16.86	4.64	48.21	1.39	3.28	6.94	0.0	nan	0.0	nan	0.0	nan
PWR19	315	4233.67	0.13	11.22	6.4	19.86	4.36	54.67	1.36	3.92	6.32	0.0	nan	0.0	nan	0.0	nan
PWR20	135	4265.93	0.13	12.46	6.0	21.41	4.27	60.82	1.28	4.2	6.18	0.0	nan	0.0	nan	0.0	nan
PWR20	225	4295.58	0.13	12.58	6.01	21.86	4.21	62.25	1.27	4.34	6.23	0.0	nan	0.0	nan	0.0	nan
PWR20	315	4190.61	0.13	11.79	6.16	21.84	4.05	58.11	1.31	4.02	6.29	0.0	nan	0.0	nan	0.0	nan
PWR21	45	4125.89	0.13	11.48	6.36	21.78	4.05	58.89	1.29	4.2	6.0	0.0	nan	0.0	nan	0.0	nan
PWR21	135	4333.87	0.13	12.47	6.12	23.05	4.05	63.69	1.25	4.24	6.42	0.0	nan	0.0	nan	0.0	nan
PWR21	315	3973.0	0.13	11.53	5.87	20.17	4.03	56.84	1.23	4.18	5.61	0.0	nan	0.0	nan	0.0	nan
PWR22	45	4008.91	0.13	10.68	6.6	19.45	4.39	56.98	1.29	4.03	7.38	0.0	nan	0.0	nan	0.0	nan
PWR22	225	3684.98	0.13	10.12	16.04	17.99	4.29	50.87	1.31	3.67	6.02	0.0	nan	0.0	nan	0.0	nan
PWR22	315	3888.19	0.13	10.42	6.36	18.27	4.34	54.13	1.26	3.83	10.83	0.0	nan	0.0	nan	0.0	nan
PWR23	45	4014.3	0.13	17.81	4.27	32.51	2.83	91.26	0.92	6.42	4.41	0.0	nan	13.17	11.08	0.0	nan
PWR23	135	4368.64	0.13	19.67	8.6	34.44	2.94	99.1	0.92	7.01	4.45	0.0	nan	14.14	11.37	0.0	nan
PWR23	225	4595.48	0.13	20.57	4.39	37.15	2.94	103.56	0.95	7.39	4.66	0.0	nan	15.44	11.25	0.0	nan
PWR23	315	4244.62	0.13	0.0	nan	34.39	2.79	95.73	0.91	7.18	4.16	0.0	nan	14.13	10.83	0.0	nan
PWR24	45	2781.1	0.15	12.39	4.68	21.39	3.29	63.1	1.03	4.47	4.61	0.0	nan	0.0	nan	0.0	nan
PWR24	135	2718.98	0.15	12.01	4.64	21.64	3.13	60.34	1.05	4.54	4.51	0.0	nan	0.0	nan	0.0	nan
PWR24	225	2972.75	0.15	13.78	4.42	24.95	2.97	68.8	1.0	4.95	4.42	0.0	nan	0.0	nan	0.0	nan
PWR24	315	3062.34	0.14	14.63	4.33	26.29	2.9	73.61	0.97	5.37	4.35	0.0	nan	0.0	nan	0.0	nan
PWR25	45	2361.83	0.16	4.91	8.27	8.86	5.56	24.72	1.74	1.91	7.09	0.0	nan	0.0	nan	0.0	nan
PWR25	135	2409.35	0.15	4.72	8.67	8.51	5.78	25.14	1.7	1.73	8.44	0.0	nan	0.0	nan	0.0	nan
PWR25	225	2323.86	0.16	0.0	nan	8.28	5.79	23.93	1.75	1.67	8.33	0.0	nan	0.0	nan	0.0	nan
PWR25	315	2288.75	0.16	0.0	nan	8.71	5.45	24.19	1.72	1.79	7.33	0.0	nan	0.0	nan	0.0	nan

Table C.17
Mean relative uncertainty calculated from Tables C.15 and C.16.

Energy [keV]	662	996	1004	1274	1596	605	796	1365
Campaign1	0.20%	5.11%	3.12%	1.02%	3.86%	3.27%	2.73%	3.27%
Campaign2	0.21%	6.33%	4.19%	1.44%	5.93%	6.21%	3.04%	5.03%

Table D.18
Calculated count per seconds for Cs-137, and the ratios Eu-154/Cs-137, and Cs-134/Cs-137, with correction for attenuation plates for campaign 2. The date is the measurement date.

Assembly	Cs-137 [cps]	Unc.[%]	Eu-154/Cs-137	Unc.[%]	Cs-134/Cs-137	Unc.[%]	Date
BWR02	2926	0.15	0.02107	1.07	0.01388	1.24	2019-03-26
BWR03	2843	2.09	0.01853	0.74	0.00683	1.78	2019-03-27
BWR05	2926	2.40	0.02249	0.48	0.02179	1.36	2019-03-27
BWR06	1426	0.70	0.00837	0.65	NaN	NaN	2019-03-27
BWR07	2739	2.44	0.02055	0.69	0.01283	1.91	2019-03-26
BWR10	2848	1.16	0.02455	0.66	0.02868	1.27	2019-03-26
BWR11	1261	2.66	0.01130	1.47	NaN	NaN	2019-03-27
BWR12	2247	0.52	0.02317	0.81	0.01649	0.43	2019-03-26
BWR13	2424	0.67	0.02355	0.69	0.01710	1.35	2019-03-27
BWR14	1146	0.70	0.00765	1.11	NaN	NaN	2019-03-28
BWR15	1128	1.10	0.00884	1.19	NaN	NaN	2019-03-28
BWR16	1010	2.30	0.00825	1.11	NaN	NaN	2019-03-27
BWR17	1163	2.16	0.00891	0.90	NaN	NaN	2019-03-28
BWR18	871	2.29	0.00992	1.65	NaN	NaN	2019-03-28
BWR19	1236	0.97	0.00965	0.52	NaN	NaN	2019-03-27
BWR21	945	1.51	0.00867	1.42	NaN	NaN	2019-03-27

(*continued on next page*)

Table D.18 (*continued*).

Assembly	Cs-137 [cps]	Unc.[%]	Eu-154/Cs-137	Unc.[%]	Cs-134/Cs-137	Unc.[%]	Date
BWR22	1406	1.63	0.01589	1.13	0.01138	2.58	2019-03-28
BWR24	471	6.36	0.00628	1.30	NaN	NaN	2019-03-27
BWR25	289	8.04	0.00434	3.41	NaN	NaN	2019-03-28
PWR01	10 872	1.14	0.04480	0.40	0.18711	0.50	2016-11-09
PWR02	10 534	1.12	0.04279	0.47	0.16337	1.35	2016-11-09
PWR04	9718	0.69	0.04008	0.65	0.11985	1.61	2016-09-28
PWR05	9704	0.95	0.03960	0.48	0.11628	1.41	2016-11-07
PWR07	8816	1.37	0.03768	0.71	0.08603	1.78	2016-09-28
PWR08	5779	0.55	0.01253	0.66	NaN	NaN	2016-11-07
PWR09	9308	1.53	0.03749	0.43	0.08828	1.27	2016-11-08
PWR10	7122	5.67	0.02174	0.70	0.00515	2.01	2016-09-27
PWR11	6744	6.99	0.02385	1.33	0.00634	9.28	2016-09-27
PWR12	5734	2.08	0.01203	0.59	NaN	NaN	2016-11-08
PWR13	4927	2.12	0.01059	0.73	NaN	NaN	2016-11-09
PWR14	6295	3.73	0.02080	0.59	0.00373	4.01	2016-09-27
PWR15	5271	2.47	0.01174	0.44	NaN	NaN	2016-09-29
PWR16	6237	1.06	0.01884	0.52	0.00241	4.39	2016-09-28
PWR17	6520	4.62	0.02336	0.49	0.00733	1.10	2016-11-08
PWR18	5653	1.65	0.01725	0.62	0.00138	nan	2016-09-28
PWR19	4059	2.95	0.00904	0.77	NaN	NaN	2016-11-08
PWR20	4249	0.74	0.01004	0.92	NaN	NaN	2016-09-29
PWR21	4130	2.52	0.01019	0.86	NaN	NaN	2016-09-29
PWR22	3853	2.44	0.00983	0.51	NaN	NaN	2016-11-08
PWR23	4283	2.80	0.01597	0.52	0.00223	0.81	2016-09-28
PWR24	2875	2.79	0.01625	1.05	NaN	NaN	2016-09-29
PWR25	2344	1.10	0.00736	0.59	NaN	NaN	2016-11-07

Table D.19
Calculated count per seconds for Cs-137, and the ratios Eu-154/Cs-137, and Cs-134/Cs-137, with correction for the attenuation plates for campaign 1. The date is the measurement date.

Assembly	Cs-137 [cps]	Unc.[%]	Eu-154/Cs-137	Unc.[%]	Cs-134/Cs-137	Unc.[%]	Date
BWR01	3543	1.00	0.02981	0.47	0.08516	0.85	2014-12-01
BWR02	3214	0.33	0.02776	0.88	0.05530	0.80	2014-12-02
BWR03	3100	1.77	0.02480	0.51	0.02649	1.23	2014-12-09
BWR04	2880	2.35	0.02529	0.26	0.02427	1.04	2014-12-09
BWR05	3240	2.16	0.02963	0.58	0.08590	1.12	2014-12-02
BWR06	1522	1.32	0.01108	1.14	NaN	NaN	2014-12-10
BWR07	3002	2.47	0.02751	0.54	0.05038	0.75	2014-12-02
BWR08	2875	1.22	0.03232	0.29	0.08464	0.57	2014-12-03
BWR09	3191	2.17	0.03100	0.34	0.11930	1.41	2014-12-02
BWR10	3134	0.92	0.03287	0.31	0.11255	0.64	2014-12-01
BWR11	1346	3.58	0.01475	1.26	0.00107	5.30	2014-12-08
BWR12	2441	1.03	0.03085	0.37	0.06383	0.71	2014-12-03
BWR13	2726	1.30	0.03176	0.47	0.06894	1.31	2014-12-02
BWR14	1207	1.84	0.00998	0.84	NaN	NaN	2014-12-10
BWR15	1181	1.05	0.01138	0.47	NaN	NaN	2014-12-09
BWR16	1097	2.11	0.01081	0.81	NaN	NaN	2014-12-09
BWR17	1255	2.09	0.01164	0.63	NaN	NaN	2014-12-04
BWR18	946	2.56	0.01301	1.54	0.00104	2.61	2014-12-08
BWR19	1338	0.17	0.01261	0.67	NaN	NaN	2014-12-04
BWR20	1988	1.15	0.02768	0.43	0.06253	1.19	2014-12-03
BWR21	1023	1.05	0.01121	0.65	NaN	NaN	2014-12-04
BWR22	1549	1.48	0.02095	0.67	0.04395	1.83	2014-12-02
BWR23	1174	3.58	0.01654	0.86	0.03685	1.95	2014-12-03
BWR24	511	5.38	0.00785	0.59	NaN	NaN	2014-12-03
BWR25	317	9.08	0.00554	2.02	NaN	NaN	2014-12-04
PWR01	12 452	1.81	0.35288	0.42	2.50847	0.63	2014-10-07
PWR02	11 688	1.25	0.34360	0.31	2.20861	1.91	2014-10-07
PWR03	9076	3.40	0.20325	0.42	0.14597	0.88	2014-10-09
PWR04	10 556	0.70	0.32749	0.40	1.56710	1.49	2014-10-09
PWR05	10 668	1.52	0.32270	0.27	1.56436	1.22	2014-10-10
PWR06	8216	1.11	0.19336	0.40	0.09973	1.49	2014-10-10
PWR07	9668	1.79	0.30437	0.54	1.11510	1.76	2014-10-10
PWR08	6330	0.87	0.10170	0.37	NaN	NaN	2014-10-13
PWR09	10 259	2.02	0.29851	0.32	1.16869	2.00	2014-10-07
PWR10	7880	3.29	0.17366	0.50	0.06666	1.98	2014-10-13
PWR11	7605	3.52	0.19170	0.64	0.08284	3.81	2014-10-13
PWR12	6382	1.75	0.09684	0.46	NaN	NaN	2014-10-15
PWR13	5368	2.24	0.08606	0.35	NaN	NaN	2014-10-08
PWR14	6970	4.51	0.16601	0.55	0.04965	1.43	2014-10-14
PWR15	5586	1.55	0.09306	0.50	NaN	NaN	2014-10-08
PWR16	6855	1.11	0.15040	0.54	0.03157	2.66	2014-10-15

(*continued on next page*)

Table D.19 (*continued*).

Assembly	Cs-137 [cps]	Unc.[%]	Eu-154/Cs-137	Unc.[%]	Cs-134/Cs-137	Unc.[%]	Date
PWR17	7287	2.32	0.19009	0.29	0.09699	1.10	2014-10-14
PWR18	6190	2.26	0.13949	0.60	0.01694	4.17	2014-10-08
PWR19	4361	3.25	0.07208	0.69	NaN	NaN	2014-10-08
PWR20	4663	0.79	0.08065	0.67	NaN	NaN	2014-10-14
PWR21	4638	0.94	0.08109	0.49	NaN	NaN	2014-10-15
PWR22	4231	2.28	0.07877	0.82	NaN	NaN	2014-10-15
PWR23	4750	2.61	0.12664	0.50	0.03216	2.40	2014-10-15
PWR24	3065	2.20	0.12836	1.14	0.01144	5.68	2014-10-09
PWR25	2489	1.38	0.05783	0.66	NaN	NaN	2014-10-13

References

Bengtsson, M., Jansson, P., Bäckström, U., Johansson, F., Sjöland, A., 2021. Experimental method for verification of calculated ^{137}Cs content in nuclear fuel assemblies. Nucl. Technol. 1–8. http://dx.doi.org/10.1080/00295450.2021.1880851, URL https://www.tandfonline.com/doi/full/10.1080/00295450.2021.1880851.

Caruso, S., Vlassopoulos, E., Dagan, R., Fiorito, L., Herm, M., Jansson, P., Kromar, M., Kiraly, M., Leppanen, J., Marquez, F., Metz, V., Papaioannou, D., Herranz, L., Rochman, D., Schillebeeckx, P., Seidl, M., Solis, A., Stankovskiy, A., Alvarez Velarde, F., Verwrft, M., Nieves Rodriguez Villagra, M., Zencker, U., Zerovnik, G., 2022. European joint programme on radioactive waste management, state of the art report. Technical report, EURAD WP8, Available from: https://www.ejp-eurad.eu/publications/eurad-deliverable-81-state-art-report.

Elter, Z., Cserkaszky, A., Grape, S., 2019. feign: a Python package to estimate geometric efficiency in passive gamma spectroscopy measurements of nuclear fuel. J. Open Source Softw. 4 (42), 1650. http://dx.doi.org/10.21105/joss.01650, URL https://joss.theoj.org/papers/10.21105/joss.01650.

Favalli, A., Vo, D., Grogan, B., Jansson, P., Liljenfeldt, H., Mozin, V., Schwalbach, P., Sjöland, A., Tobin, S., Trellue, H., Vaccaro, S., 2016. Determining initial enrichment, burnup, and cooling time of pressurized-water-reactor spent fuel assemblies by analyzing passive gamma spectra measured at the Clab interim-fuel storage facility in Sweden. Nucl. Instrum. Methods Phys. Res. A 820, 102–111. http://dx.doi.org/10.1016/j.nima.2016.02.072, URL https://linkinghub.elsevier.com/retrieve/pii/S0168900216002485.

Hartung, J., Knapp, G., Sinha, B.K., 2008. Statistical Meta-Analysis with Applications. In: Wiley series in probability and statistics, Wiley, Hoboken, N.J, oCLC: ocn212627347.

Hellesen, C., Grape, S., Jansson, P., Jacobsson Svärd, S., Åberg Lindell, M., Andersson, P., 2017. Nuclear spent fuel parameter determination using multivariate analysis of fission product gamma spectra. Ann. Nucl. Energy 110, 886–895. http://dx.doi.org/10.1016/j.anucene.2017.07.035, URL https://linkinghub.elsevier.com/retrieve/pii/S0306454917302220.

Jansson, P., Bengtsson, M., Bäckström, U., Álvarez-Velarde, F., Čalič, D., Caruso, S., Dagan, R., Fiorito, L., Giot, L., Govers, K., Hernandez Solis, A., Hannstein, V., Ilas, G., Kromar, M., Leppänen, J., Mosconi, M., Ortego, P., Plukienė, R., Plukis, A., Ranta-Aho, A., Rochman, D., Ros, L., Sato, S., Schillebeeckx, P., Shama, A., Simeonov, T., Stankovskiy, A., Trellue, H., Vaccaro, S., Vallet, V., Verwerft, M., Žerovnik, G., Sjöland, A., 2022. Blind benchmark exercise for spent nuclear fuel decay heat. Nucl. Sci. Eng. 1–21. http://dx.doi.org/10.1080/00295639.2022.2053489, URL https://www.tandfonline.com/doi/full/10.1080/00295639.2022.2053489.

Jansson, P., Bengtsson, M., Bäckström, U., Grape, S., Branger, E., Sjöland, A., 2020. Time stamped list mode data from gamma-ray spectroscopic measurements on 47 nuclear fuel assemblies performed at Clab, Sweden, September 2016 through March 2019. Data Brief 31, 106039. http://dx.doi.org/10.1016/j.dib.2020.106039, URL https://linkinghub.elsevier.com/retrieve/pii/S2352340920309331.

Jansson, P., Tobin, S., Liljenfeldt, H., Fugate, M., Favalli, A., Sjöland, A., 2016. Axial and azimuthal gamma scanning of nuclear fuel - implications for spent fuel characterization. J. Nucl. Mater. Manage. 45 (1), 34–47, URL https://resources.inmm.org/system/files/jnmm/vol_45/V-45_1.pdf.

Knoll, G.F., 1989. Radiation Detection and Measurement, second ed. Wiley, New York.

Sadawy, M., El Shazly, R., 2019. Nuclear radiation shielding effectiveness and corrosion behavior of some steel alloys for nuclear reactor systems. Def. Technol. 15 (4), 621–628. http://dx.doi.org/10.1016/j.dt.2019.04.001, URL https://linkinghub.elsevier.com/retrieve/pii/S2214914718305476.

Sampson, T.E., Kelley, T.A., Vo, D.T., 2003. Application Guide to Gamma Ray Isotopic Analysis, p. 177.

Seltzer, S., 1995. Tables of X-ray mass attenuation coefficients and mass energy-absorption coefficients, NIST standard reference database 126. National Institute of Standards and Technology, http://dx.doi.org/10.18434/T4D01F, type: dataset, URL http://www.nist.gov/pml/data/xraycoef/index.cfm.

Solans, V., Rochman, D., Brazell, C., Vasiliev, A., Ferroukhi, H., Pautz, A., 2021a. Optimisation of used nuclear fuel canister loading using a neural network and genetic algorithm. Neural Comput. Appl. 33 (23), 16627–16639. http://dx.doi.org/10.1007/s00521-021-06258-2, URL https://link.springer.com/10.1007/s00521-021-06258-2.

Solans, V., Sjostrand, H., Jansson, P., Grape, S., Schillebeeckx, P., Sjoland, A., 2021b. Evaluating peak area uncertainties in connection to passive gamma measurements of spent nuclear fuel. URL https://az659834.vo.msecnd.net/eventsairwesteuprod/production-ens-public/4bd8b685fec04d77b065956106a57434.

Trahan, A.C., McMath, G.E., Mendoza, P.M., Trellue, H.R., Backstrom, U., Balkeståhl, L.P., Grape, S., Henzl, V., Leyba, D., Root, M.A., Sjoland, A., 2020. Results of the Swedish spent fuel measurement field trials with the Differential Die-Away Self-Interrogation Instrument. Nucl. Instrum. Methods Phys. Res. A 955, 163329. http://dx.doi.org/10.1016/j.nima.2019.163329, URL https://linkinghub.elsevier.com/retrieve/pii/S0168900219315621.

Vaccaro, S., Tobin, S.J., Favalli, A., Grogan, B., Jansson, P., Liljenfeldt, H., Mozin, V., Hu, J., Schwalbach, P., Sjöland, A., Trellue, H., Vo, D., 2016. PWR and BWR spent fuel assembly gamma spectra measurements. Nucl. Instrum. Methods Phys. Res. A 833, 208–225. http://dx.doi.org/10.1016/j.nima.2016.07.032, URL https://www.sciencedirect.com/science/article/pii/S0168900216307707.

Virtanen, P., Gommers, R., Oliphant, T.E., Haberland, M., Reddy, T., Cournapeau, D., Burovski, E., Peterson, P., Weckesser, W., Bright, J., van der Walt, S.J., Brett, M., Wilson, J., Millman, K.J., Mayorov, N., Nelson, A.R.J., Jones, E., Kern, R., Larson, E., Carey, C.J., Polat, I., Feng, Y., Moore, E.W., VanderPlas, J., Laxalde, D., Perktold, J., Cimrman, R., Henriksen, I., Quintero, E.A., Harris, C.R., Archibald, A.M., Ribeiro, A.H., Pedregosa, F., van Mulbregt, P., SciPy 1.0 Contributors, Vijaykumar, A., Bardelli, A.P., Rothberg, A., Hilboll, A., Kloeckner, A., Scopatz, A., Lee, A., Rokem, A., Woods, C.N., Fulton, C., Masson, C., Häggström, C., Fitzgerald, C., Nicholson, D.A., Hagen, D.R., Pasechnik, D.V., Olivetti, E., Martin, E., Wieser, E., Silva, F., Lenders, F., Wilhelm, F., Young, G., Price, G.A., Ingold, G.-L., Allen, G.E., Lee, G.R., Audren, H., Probst, I., Dietrich, J.P., Silterra, J., Webber, J.T., Slavič, J., Nothman, J., Buchner, J., Kulick, J., Schönberger, J.L., de Miranda Cardoso, J.V., Reimer, J., Harrington, J., Rodríguez, J.L.C., Nunez-Iglesias, J., Kuczynski, J., Tritz, K., Thoma, M., Newville, M., Kümmerer, M., Bolingbroke, M., Tartre, M., Pak, M., Smith, N.J., Nowaczyk, N., Shebanov, N., Pavlyk, O., Brodtkorb, P.A., Lee, P., McGibbon, R.T., Feldbauer, R., Lewis, S., Tygier, S., Sievert, S., Vigna, S., Peterson, S., More, S., Pudlik, T., Oshima, T., Pingel, T.J., Robitaille, T.P., Spura, T., Jones, T.R., Cera, T., Leslie, T., Zito, T., Krauss, T., Upadhyay, U., Halchenko, Y.O., Vázquez-Baeza, Y., 2020. SciPy 1.0: fundamental algorithms for scientific computing in Python. Nature Methods 17 (3), 261–272. http://dx.doi.org/10.1038/s41592-019-0686-2, URL http://www.nature.com/articles/s41592-019-0686-2.